Anatomy of the bi-gradational contourite sequence: Case study from the Gulf of Cadiz

Dorrik Stow [a,*], Zeinab Smillie [a], Jonathan Wilkin [b], Jiawei Pan [a], Onoriode Esegbue [c], André Bahr [d], Emmanuelle Ducassou [e]

[a] Heriot-Watt University, Edinburgh, Scotland, United Kingdom
[b] University of Dundee, Dundee, Scotland, United Kingdom
[c] University of Newcastle, Newcastle upon Tyne, England, United Kingdom
[d] Heidelberg University, D-69120 Heidelberg, Germany
[e] Université de Bordeaux, Bordeaux, France

ARTICLE INFO

ABSTRACT

The bi-gradational sequence (C1-C5) is the standard facies model for fine-grained, mixed mud-sand contourites. Drilling in the Gulf of Cadiz during IODP 339 recovered over 4.5 km of contourites with over 1600 distinct contourite sequences, having an average thickness of 3 m (range 0.5–7.5 m). This study documents the past 1.1 My of contourite succession at IODP Site U1389, in which there are a total of 299 full and partial sequences, with a variable thickness of 0.13–10.6 m (mean 2.65 m) and estimated duration of 0.4–32 ky (mean 8 ky).

Two complete bi-gradational sequences have been analysed in detail. Primary sedimentary structures are absent, apart from some bedding-parallel sharp contacts and abrupt omission surfaces. Bioturbation is pervasive throughout, and a distinctive pattern of ichnofacies change is observed through each sequence. Textural trends show reverse to normal bi-gradation through the sequence: mean size ranges from 7 μm to 55 μm, sorting from 1.8 to 2.9 phi, skewness from −0.3 to +0.6, and kurtosis from mesokurtic to very platykurtic. Compositional trends based on mineralogy, inorganic and organic geochemistry vary systematically with mean size. Of the biogenic fraction, the proportion of foraminifera increases with mean size and dominates the coarsest fraction (>150 μm). There is no discernable trend in planktonic/benthic ratio, and the benthic foraminifera are all characteristic of the upper bathyal zone. Between 30 and 60% of the tests are broken. Both terrestrial and marine sources of organic matter are present, with the former more abundant after 1 Ma and the latter dominant from 2 to 1 Ma.

Collectively, these facets of the contourite sequence validate the dual controls exerted by long-term variation in bottom-current velocity and episodic changes in sediment supply (both clastic and biogenic). Of these, bottom current velocity is the more important. Estimates of bottom current speeds, based on the standard sortable silt (SS) proxy, for the two sequences range from approximately 12–24 cm s^{-1} (with fluctuations of 1–5 cm s^{-1}). However, we would support the case for a refined method that takes into account the very fine sand fraction moved by bottom currents. Where current speed is relatively high then non-deposition/erosion occurred and an omission surface results. Such omission surfaces probably account for between 20% and 35% of missing section in the two studied sequences. Where current speed was relatively low, thick featureless mud is deposited with a dominant hemipelagic sediment supply and slow alongslope drift. Such hybrid contourite-hemipelagite muds are believed to be widespread in the ocean.

1. Introduction

The early pioneering work on contourites led to two very contrasting models for contourite sediments – very thin-bedded rippled silts and sands (Hollister and Heezen, 1972) versus thoroughly bioturbated muddy silts and muddy sands with poorly-defined bedding (Stow, 1977, 1979). Further work on many drift systems worldwide led to a resolution of these differences, and the recognition that many of the thin-bedded

sands originally described by Hollister were, in fact, bottom-current reworked turbidites or fine-grained turbidites, and that the interbedding of bioturbated muds, silts and muddy sands were more typical of large fine-grained drift systems (Hollister, 1993; Stow and Faugères, 2008). The two facies models then established for muddy and sandy contourites (Stow and Lovell, 1979; Stow, 1982) were later combined into the now standard mud-sand-mud, bi-gradational facies model (Faugères et al., 1984; Gonthier et al., 1984; Stow and Piper, 1984).

The C1 to C5 notation was added later to the bi-gradational model (Stow et al., 2002), and the range of partial sequences, mud-rich and sand-rich variations encountered in contourite successions were outlined by Stow and Faugères (2008) (Fig. 1). This model of complete and partial sequences for fine-grained (mud-rich and mixed sand-mud) contourites represents most but not all of the spectrum of contourite facies. Sandy contourites, for example, occur as part of bi-gradational sequences and also separately (Capella et al., 2017; Brackenridge et al., 2018; Stow and Smillie, 2020). In this latter case they are more sharply interbedded with muddy contourites rather than showing gradational contacts. Mud-only contourites (C1-C5) occur in large open-ocean muddy drifts and in thick muddy sections of mixed drifts. These are part of a gradational facies continuum into hemipelagites.

Drilling in the Gulf of Cadiz during IODP 339 recovered over 4.5 km of contourites with over 1600 distinct contourite sequences recorded during shipboard logging (Stow et al., 2013). In a companion paper, Pan et al. (2022) use a geostatistical approach to analyse the nature and repetition of contourite sequences over a total of 1460 m of section at two IODP sites 1386 and 1387 in the Gulf of Cadiz. They noted clear bi-gradational sequences (0.5–5 m thick) for the past 1.4 Ma, but with marked variation in thickness and complexity. There is good correlation of sequences between sites, but not a perfect match for every sequence.

Further analyses have focused on the textural characteristics of contourites at these and other sites (Brackenridge et al., 2018; Yu et al., 2020), and on composition, geochemistry and grain size distinction from turbidites and hemipelagites (Alsonso et al., 2016; de Castro et al., 2020). Their link to petrophysical log records, correlation between different sites and a strong astronomical control (precession and eccentricity) on cyclicity was documented by Lofi et al. (2016).

This study focuses on the nature and sequences at IODP Site U1389, their general structure and bioturbation together with detailed measurement of sediment texture and composition of two characteristic bigradational sequences. We use these data to confirm contourite deposition; to infer the principal controls on the contourite bi-gradational sequences; and to discuss probable current speed and its variability that is responsible for deposition of such contourite sequences.

2. Study area

The Gulf of Cadiz (Fig. 2A) has been well studied over the past four decades, including the IODP Expedition 339 that focussed in particular on contourite sedimentation related to the Mediterranean Outflow Water (Stow et al., 2013; Hernández-Molina et al., 2014, 2016). The Gulf of Cadiz straddles the boundary between the African and Eurasian continental plates. It is currently in a compressional tectonic regime yielding convergence coupled with oblique WNW-ESE motion (Rosenbaum et al., 2002). The continental margin along the northern Gulf of Cadiz is broadly arcuate, approximately 350 km long, and runs from the Strait of Gibraltar to the south-western tip of Portugal (Cape St Vincent) (Fig. 2). Morphological features of the continental slope demonstrate both downslope and alongslope processes, with a dominant imprint of alongslope bottom-current activity on the mid-slope region between 400 and 1500 m water depth (Hernández-Molina et al., 2006; Medialdea et al., 2009).

This bottom-current activity is the result of water exchange between the Atlantic Ocean and Mediterranean Sea through the Strait of Gibraltar (or *Gibraltar Gateway*), which involves the overflow of warm saline Mediterranean Outflow Water (MOW) at depth and the surface influx of Atlantic Inflow Water (AIW) (Howe, 1982; Baringer and Price, 1999; Lobo et al., 2000; Ambar et al., 2002; Cabecadas et al., 2002; Garcia-Lafuente et al., 2006; Llave et al., 2007). The Mediterranean Outflow is intensified through the relatively narrow Gibraltar Gateway, reaching velocities up to 300 cm s^{-1} (Ambar and Howe, 1979; Mulder et al., 2003) as it cascades over the shallow sill, causing turbulence, meso-scale eddies and seafloor erosion. It then veers towards the northwest as a result of the Coriolis Effect and separates into several distinct strands as
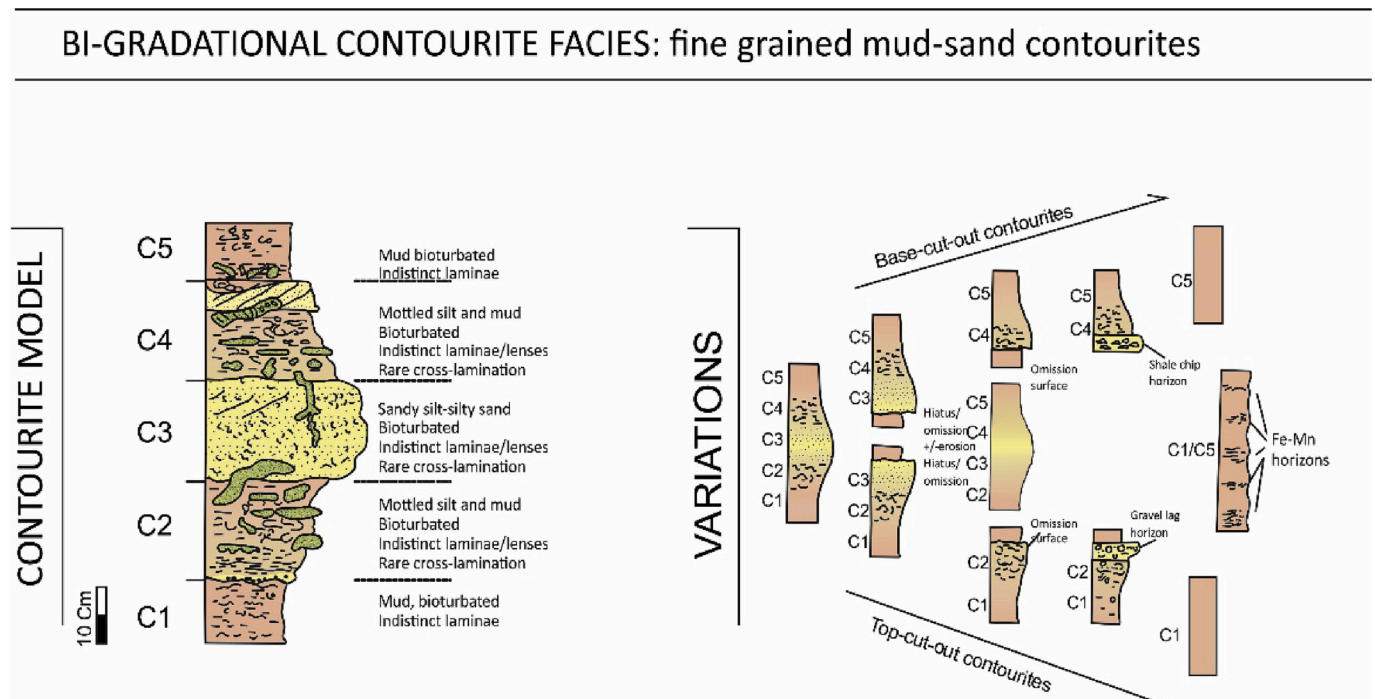

Fig. 1. Standard contourite bi-gradational sequence model and typical variations in nature (Stow and Smillie, 2020).
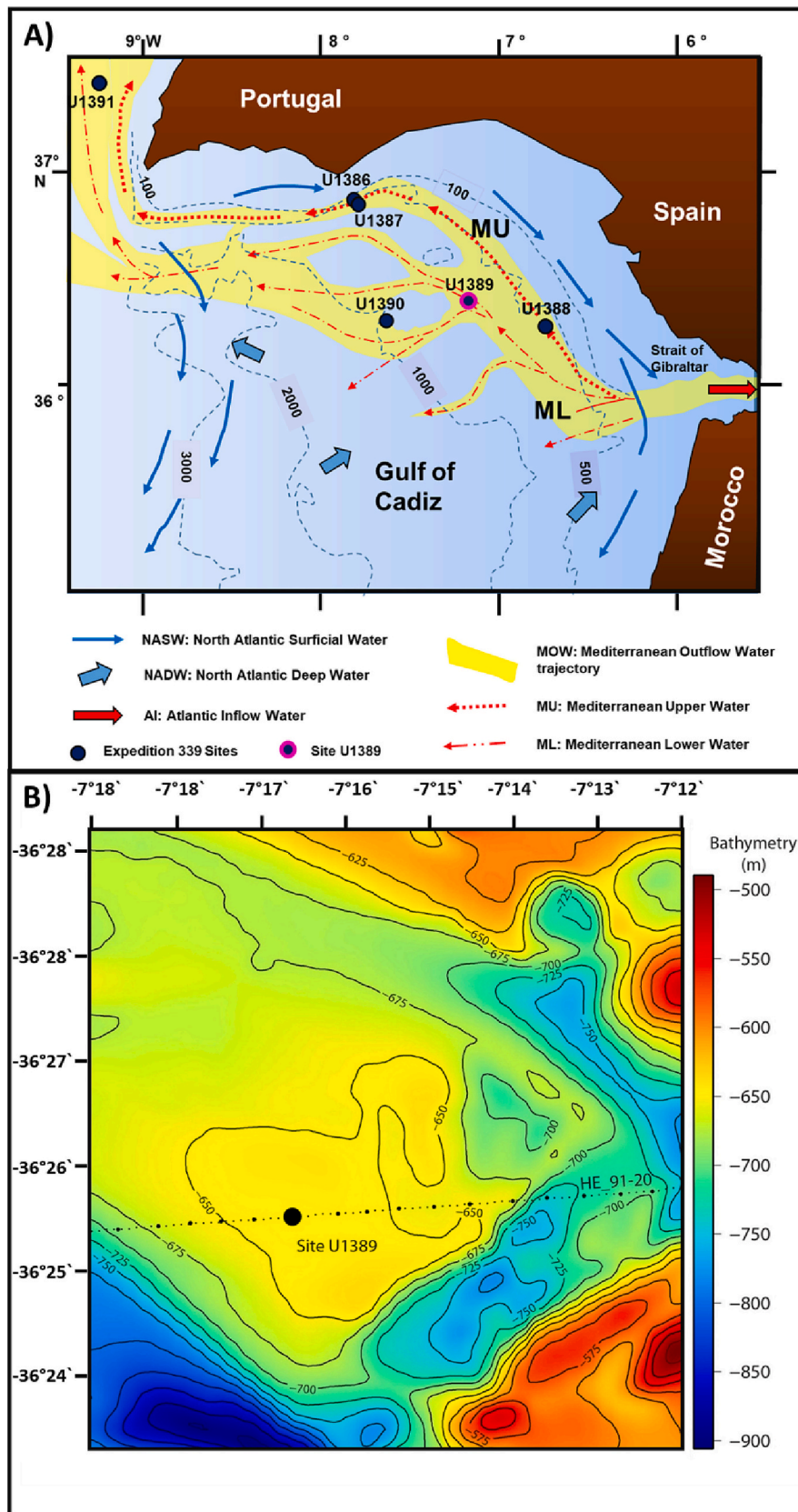
Fig. 2. (A) Gulf of Cadiz study area showing pathway of present-day Mediterranean Outflow Water (MOW) and location of IODP 339 sites (after Hernández-Molina et al., 2016). (B) Location of site 1389 (this study) with detailed bathymetry showing a sheeted drift surrounded by contourite channels (from Stow et al., 2013).

it interacts with diapiric-induced seafloor topography (Fig. 2). The MOW leaves the seabed as it reaches a neutral buoyancy at a depth of 1200–1400 m (Zenk, 1975; Ambar et al., 1999; Rogerson et al., 2005).

Separation of the MOW into different strands has led to the erosion of nine distinct contourite channels along the northern Cadiz continental slope (García et al., 2009). Site U1389 is located on a partially isolated sheeted drift between two of these channels – the northern branch of the Guadalquivir Contourite Channel, the Huelva Contourite Channel and a marginal valley adjacent to the Guadalquivir Diapiric Ridge (Figs. 2B, 3). The site has therefore been isolated from downslope turbidity currents, but subjected to the likely interference between different strands of the MOW. Contourite sedimentation and erosion under this current regime began in the early Pliocene (Stow et al., 2013; Hernández-Molina et al., 2014, 2016; Bahr et al., 2015).

3. Methodology

3.1. Sequence selection and logging

Five holes were drilled at Site U1389, four of which (A-D) penetrated part or all of the Holocene to mid-Pleistocene succession, and were examined for this study (Fig. 3). Hole U1389E was initiated within the early Pleistocene and extends to the mid-Pliocene at around 3.5 Ma. We carried out a detailed lithological log of the upper 350 m of section in U1389A with continuous recovery extending over about 1.1 My, and documented all contourite sequences observed. Two representative sequences were selected for detailed analysis, located at depths of 91 and 220 m below seafloor within cores 11H and 25X respectively. They are referred to as sequences 11H and 25X. In each case, around 5 m of section was sampled with a sampling interval of 5–20 cm.

3.2. Textural analysis

A total number of 96 samples were analysed for bulk grain size from the two selected sequences, using a Malvern Mastersizer laser microgranulometer (Malvern Panalytical) at the University of Bordeaux, France. The instrument is designed to measure the grain size spectrum ranging from 0.02 to 2000 µm (clay to sand). Grain-size statistical parameters were calculated using Gradistat software (Blott and Pye, 2001) and based on the geometric graphical method (Folk and Ward, 1957). The same samples were then treated to remove the biogenic carbonate and siliceous components, and re-analysed with the laser microgranulometer, with a view to determining the sortable silt component.

3.3. Compositional analysis

Shipboard compositional analyses included smear slide petrography, X-Ray Diffraction for bulk and clay mineralogy, and carbon-carbonate elemental analysis (Stow et al., 2013). A further set of 48 samples was subsequently analysed for organic carbon (TOC), $CaCO_3$ and stable isotopic contents, using Elemental Analyser - Isotope Ratio Mass Spectrometry (EA-IRMS). These analyses were carried out at the Iso-Analytical labs, Wales. Nine samples received duplicate analysis, one sample was duplicated every 5 runs, indicating possible analytical error within $<0.2‰$ for the $\delta^{13}C_{carb}$ and $< 0.15‰$ for both the $\delta^{13}C_{org}$ and $\delta^{18}O$. Standard reference materials were used for the $\delta^{13}C_{org}$, $\delta^{18}O$ and carbonate isotopes analyses.

Carbonate contents were extracted through acidification of the sample with 2 M hydrochloric acid, drying and weighing the sample to calculate the weight loss. Total ion beam data was used to determine the carbon percent of the acid washed samples. The weight loss data recorded at the acid washing stage was used to calculate the TOC% values from the carbon percentages.

4. Results

4.1. Facies and sequences

The contourite succession in all four holes studied from Site U1389 is dominated by fine-grained bioturbated calcareous silty muds. Six facies are identified based on slight grain-size differences: clayey mud, silty mud, sandy mud, sandy silt, silty sand and sand. Clayey mud and silty mud are the most abundant, whereas silty sand and sand are very rare. Mud is the most common field/lab term used to describe admixtures of clay, silt and sand, where the clay percentage is 25–75% of the total sediment (following the mudrock classification of Stow, 2005). Because mud is the dominant facies recorded throughout Site U1389, this is further subdivided into clayey mud (mean size 4–16 µm), silty mud (mean size 16–32 µm), sandy mud and sandy silt (mean size 32–64 µm), and silty sand or sand (mean size >64 µm). Visual inspection of the facies stacking patterns reveals coarsening-up to fining-up bi-gradational sequences, mostly with gradational contacts between individual facies, as well as various less regular facies stacking patterns (Fig. 4).

At Site U1389, we counted 299 sequences in the four holes, with continuous core recovery in Holes A and C to a depth of 350 m (Table 1, Figs. 3, 4). In these two holes, the average sequence thickness is 2.85 m and 2.63 m respectively (maximum 10.59 m, minimum 0.22 m). In calculating sequence thickness, the mud facies between successive silty to sandy facies (C2-C4 divisions) is divided exactly in half and attributed to C5 and C1 divisions respectively from base upwards. With a mean sedimentation rate of around 35 cm/ky, based on linear averaging from shipboard biostratigraphic data (Stow et al., 2013), this yields a mean sequence duration of close to 8 ky.

The coarsening-up to fining-up facies stacking is equivalent to the idealised contourite bi-gradational sequence model (Stow et al., 2002; Stow and Smillie, 2020) (Fig, 1, Fig. 5A). The clayey mud facies equates to C1 and C5 divisions, the silty and sandy mud facies equate to C2 and C4 divisions, and the sandy silt, silty sand and sand facies equate to C3 division. Several different sequence types are recorded in this study, as illustrated in Fig. 4: complete sequences, top-cut-out and base-cut-out partial sequences, mid-cut-out partial sequences and complex sequences that are more poly-gradational in nature. A typical bi-gradational sequence from Site U1389 and the two complete sequences (C1, C2, C3, C4, C5) selected for detailed analysis are illustrated in Fig. 5.
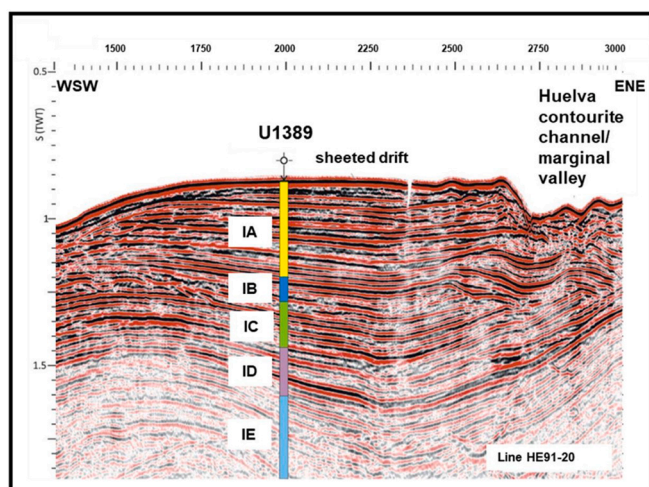

Fig. 3. (A) Seismic section across the 1389 sheeted drift site; line of section shown on Fig. 2A. (B) Summary lithology for IODP 339 Site U1389. Note shipboard lithological units designated for this site. Unit IA is the primary focus of this study (from Stow et al., 2013).
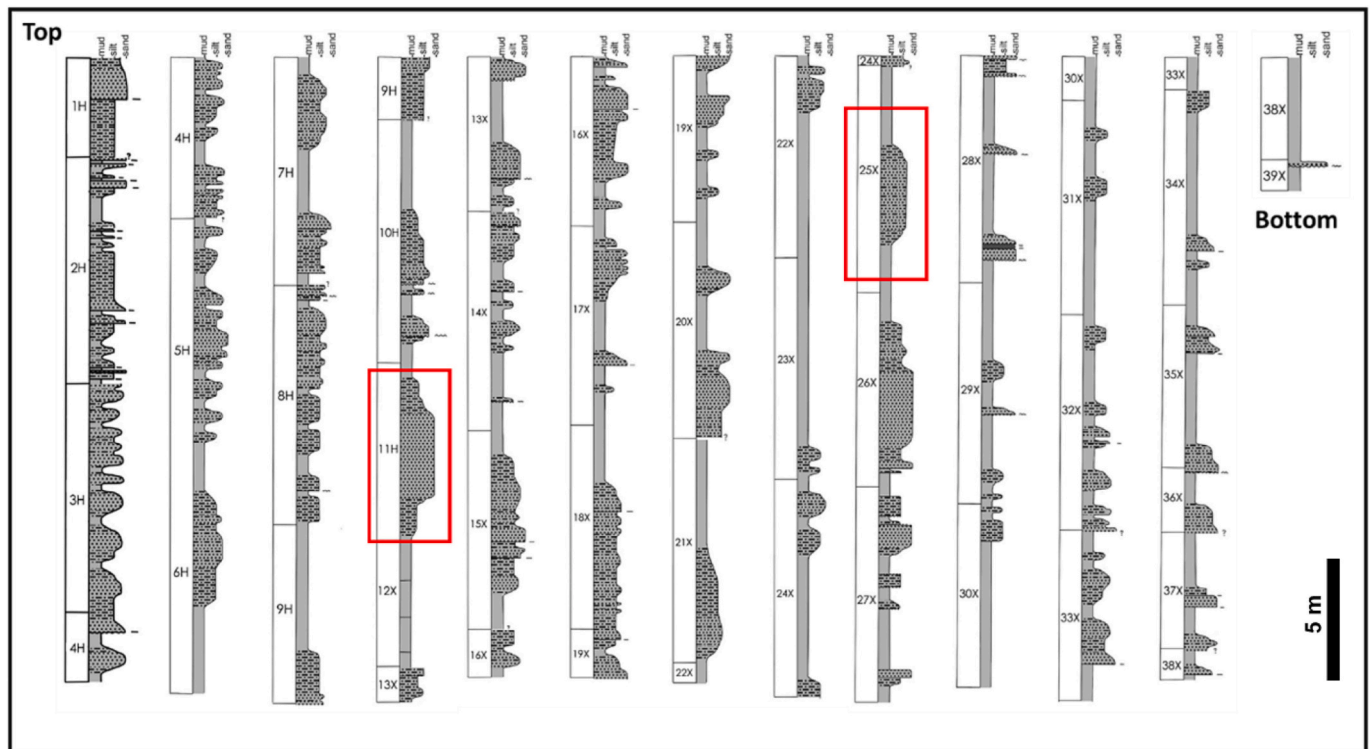
Fig. 4. Sedimentary logs through site 1389A, showing the range of sequence types and thicknesses. The two bi-gradational sequences selected for study are highlighted. The stippled ornament represents sand and silty sand; the dash-dot ornament represents sandy silt and sandy mud; and the plain grey represents the clayey mud and silty mud facies.

Table 1

Depth, age and sequence statistics for the four holes studied at Site U1389. Units, age estimates and average sedimentation rates based on shipboard data (Stow et al., 2013).

Hole	U1389A	U1389B	U1389C	U1389D
Total depth (m)	350.86	9.72	347.01	94.52
Total sequences	123	4	132	40
Unit IA	112	4	130	40
Unit IB	11	0	2	0
Average sequence thickness (m)	2.85	2.43	2.63	2.36
Maximum sequence thickness (m)	10.59	3.5	10.48	7.89
Minimum sequence thickness (m)	0.25	1.59	0.23	0.13
Variance sequence thickness (m)	5.59	0.78	5.2	3.39
Mud layers	123	4	131	40
Silty mud layers	179	5	160	55
Sandy mud layers	99	0	44	25
Sandy silt layers	1	1	0	0
Silty sand layers	43	1	45	5
Sand layers	2	1	1	0
Age covered (ky)	964.6	15.1	1064.9	288.7
Average sedimentation rate (m/ky)	0.36	0.55	0.33	0.24
Average sequence duration (ky)	7.84	3.76	8.06	10.66

4.2. Sedimentary structures and bioturbation

The upper 350 m of logged section is characterised by very uniform homogeneous olive grey (10Y 4/1) sediment, in which bedding is mostly indistinct and primary sedimentary structures are poorly preserved or completely absent (Fig. 5). There are subtle changes in grain size yielding the bi-gradational sequences noted above. Most of these sequences have gradational contacts, but some contacts are sharper; these occur at the base and tops of partial sequences, as well as within sequences where they mark minor erosion and/or omission surfaces. These represent short breaks in sedimentation of unknown duration. They may be due to an absence of sediment supply or an increase in current strength to prevent deposition, and may be accompanied by minor erosion.

Although there is no distinct lamination present, there is irregular layering and lenticularity (mm to cm-scale) present in places, especially in the muddy silt and fine sand facies. Lenses and layers may have sharp sub-horizontal contacts at top and base. In these coarser-grained facies, the omission surfaces are also more common.

Bioturbation is pervasive throughout, showing slight to moderate intensity (Fig. 5C). The mud-rich facies display millimetric-scale bioturbational mottling, and a relatively low diversity of small-size ichnofossils, including *Chondrites, Trichichnus, Mycelia,* and *Phycosiphon,* and rare larger traces of *Planolites.* Pyritisation of some of these burrows is common. The sand-rich facies displays millimetric to centimetric bioturbation, with a medium to high diversity of ichnofossils, including common *Planolites* and *Thalassinoides,* as well as some traces of *Scolicia, Skolithos, Teichichnus* and *Gyrolithes.*

These changes in ichnofacies size and diversity from muddy to sandy facies are evident through the two sequences selected for detailed study, although the full range of ichnofossils is not observed. Most typical is a rather indistinct small-scale bioturbational mottling in the mud-rich facies, and a larger-scale bioturbation with *Planolites* and *Thalassinoides* in the silt/sand-rich facies. Omission surfaces are more common in the silt/sand facies, and typically have vertical pipe and tube-like burrows extending 5–20 mm downwards. These include *Glossifungites* and *Trichichnus.* Also noted in vertical life-position below presumed omission surfaces are scaphopod macrofossils (*Arenarias* spp., Fig. 5D).

4.3. Sediment texture

4.3.1. Contourite succession

The mud-rich nature of the contourite succession at Site U1389 is typical of many fine-grained drift systems globally (Stow et al., 2008, 2018). Clay, silt and sand (mostly fine and very fine) sizes are dominant throughout. Of the measured section, <3% can be classified as a sand or
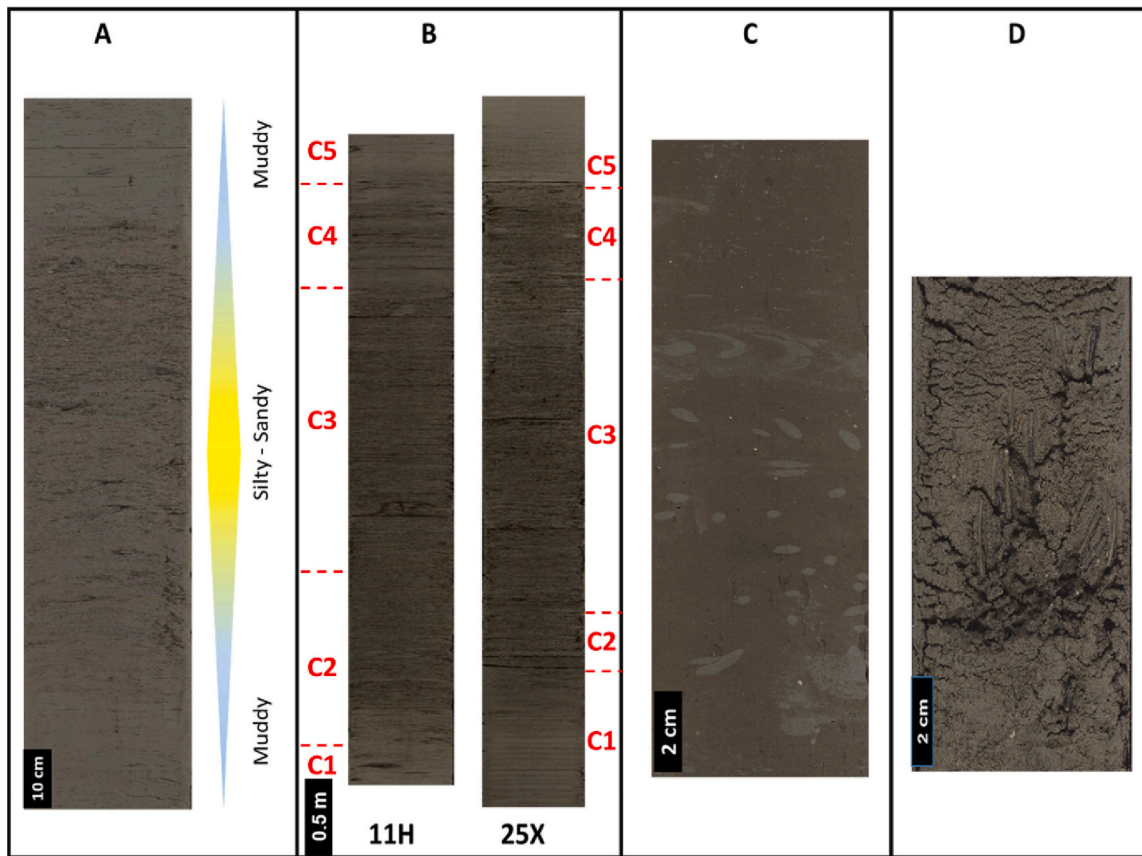
Fig. 5. Core photos of contourite facies. (A) Typical bi-gradational sequence from Site U1389. (B) The two sediment sequences detailed in this study (11H & 25×). (C) Bioturbation within the contourite sediments (Core 1389E-58, Section 3, depth 32–48 cm). (D) Silty mud contourite facies with scaphopod (*Arenarias* spp.) macrofossils in life position below presumed omission surfaces (Core 1389–13, Section 5, depth 78–88 cm).
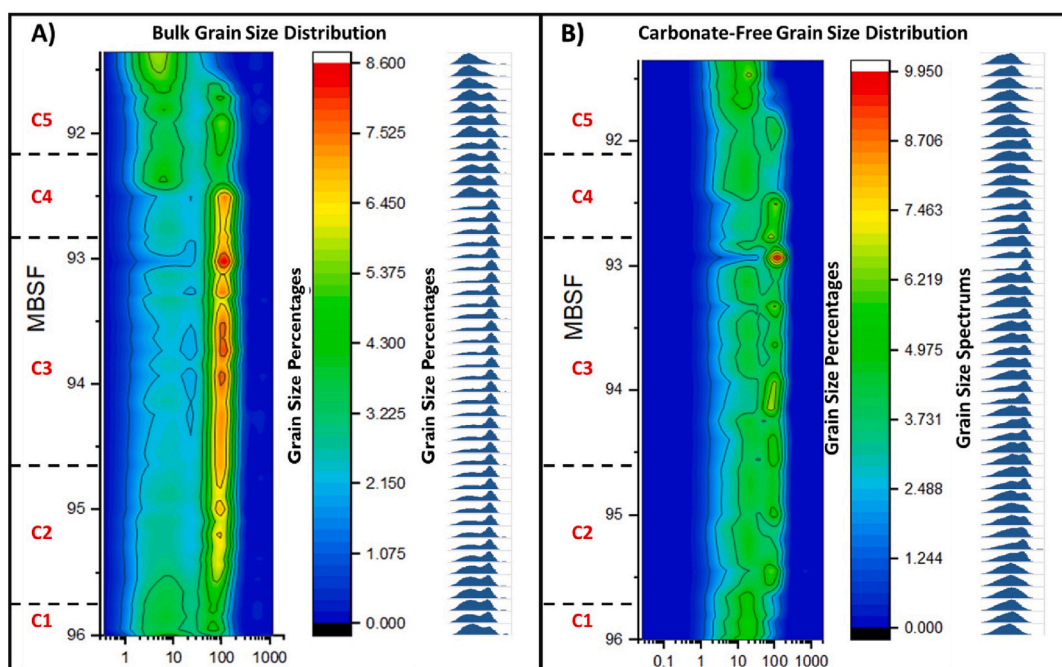

Fig. 6. Heatmap showing relative percentage of grain sizes within Sequence 11H. (A) bulk grain size distribution, and (B) carbonate-free grain size distribution after the removal of carbonate fraction. Grain size distribution spectra are displayed to the right of the heatmaps (blue plots). Note the decrease in the sand fraction contents in C3 after the removal of the carbonates. Also, the decrease in general variation in grain sizes among the different parts of the sequence when the carbonate fraction is removed. (For interpretation of the references to colour in this figure legend, the reader is referred to the web version of this article.)

silty sand facies. It should be noted that some drifts, especially in the open ocean, have even less sand and silt, although others show good foraminiferal sands. The sediments at Site U1389 are poorly or very poorly sorted. They are arranged in sequences (indistinct beds) with gradational boundaries between different facies, from which we identify the C1-C5 contourite divisions. Detailed grain size variation through the two selected sequences (11H and 25X) are documented below (Figs. 6, 7).

4.3.2. Sequence 11H

Grain size heatmaps for both the bulk sample and carbonate-free fraction are shown in Fig. 6 A & B, together with the C1 to C5

divisions and grain-size distribution spectra for 48 samples through sequence 11H (approximately 10 cm sample interval). These show that C1 and C5 are enriched in clay to very fine silt, C2 and C4 have a broader spectrum of grain sizes (silt to very fine sand), and C3 is enriched in very fine to fine sand (Fig. 6 A). The grain size changes appear to be mainly gradational between divisions, but also show oscillation every 20–50 cm, which is particularly marked through the sandy C3 division. However, in some places there are more abrupt grain size changes, which we call omission surfaces. There is one prominent omission surface in the 11H sequence at 92.5 mbsf. Further minor omission surfaces are apparent in other parts of the succession, especially in C4 and C3 divisions.
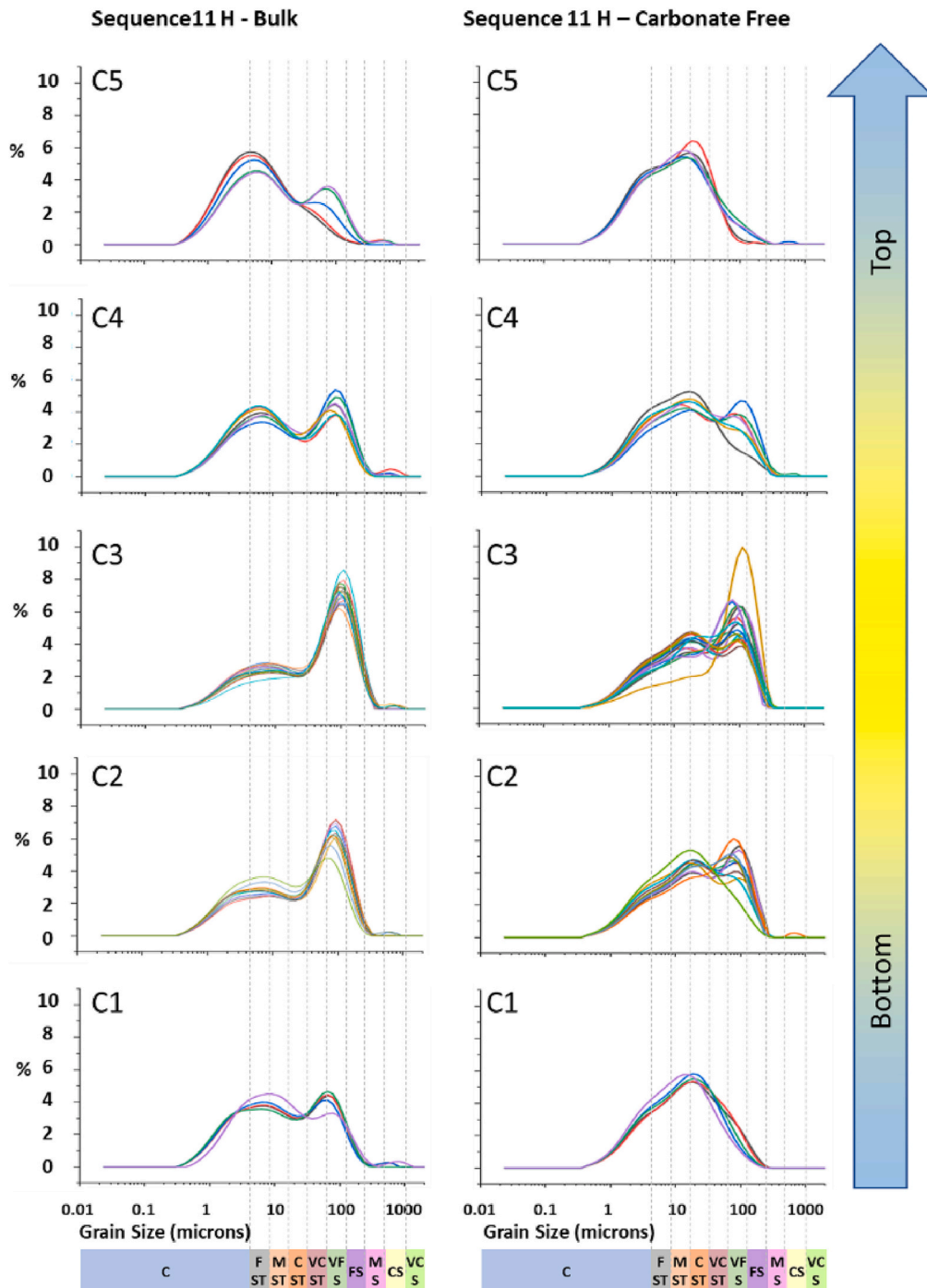

Fig. 7. Grain size distribution spectra of samples taken from the C1 to C5 divisions of sequence 11H. Division depths are: C1 = 96–95.75 mbsf, C2 = 94.65–95.65 mbsf, C3 = 94.4–92.5 mbsf, C4 = 91.7–92.4 mbsf and C5 = 91.65–91.35 mbsf.

Changes from the broad poorly-sorted grain-size distribution in the finer divisions towards a poorly-sorted bi-modal distribution in the silt-rich divisions and a more unimodal pattern in in the sandy silts can also be observed in the grain size distribution spectra shown to the right side of the heatmaps. These grain size spectra closely follow the patterns observed in heatmaps (Fig. 7). In the bulk sample plots, C1 and C5 have a prominent very fine mode (5–8 μm), and a less prominent secondary mode (60 μm). For C2 and C4, the same two modes are present but with reversed prominence and slightly coarser silt-sand mode (60–80 μm). C3 is more unimodal with a prominent mode at 100 μm, and a broader spread of silt to clay grain sizes.

Individual grain size populations are plotted separately in Fig. 8. These show a clear oscillation in grain size in all divisions, as well as distinction between divisions. When added together, C1 and C5 have 20–40% clay, 50–55% silt and minor sand; C2 and C4 have 40–50% silt, 25–40% sand and 20–25% clay; and C3 has 35–45% silt, 40–55% sand and minor clay. For the clay fraction and all the separate sand fractions, the carbonate-free percentages are lower than the bulk measurements, indicating removal of very fine carbonate fraction (nannofossils), especially in C1 and C5 divisions, and removal of the coarse carbonate fraction (foraminifera), especially in the C3 division.

The carbonate-free measurements show similar trends and patterns as for the bulk samples, with especially pronounced grain size oscillation in the sand fractions and C3 division, but with generally more muted appearance in the clay and silt fractions. The bi-gradational sequence is evident but neither so fine in the muddy divisions, nor so coarse in the sandy division. The grain size spectra (Fig. 6) show a decrease in the size of both coarser and finer modes, or their complete removal.

4.3.3. Sequence 25X

Grain size heatmaps for both the bulk sample and carbonate-free fraction are shown in Fig. 9 A & B, together with the C1 to C5 divisions and grain-size distribution spectra for 48 samples through sequence 25X (approximately 10 cm sample interval). These show an almost identical pattern to those for sequence 11H, but with slightly coarser silt and sand divisions (C2-C3-C4) with more omission surfaces, and slightly finer C1 and C5 divisions. The prominent modes for the bulk samples are 3–6 μm (C1, C5), 70–100 μm (C2, C4) and 100–125 μm (C3) (Fig. 10).

Individual grain size populations are plotted separately in Fig. 11. As for sequence 11H, these show marked oscillation in grain size in all divisions, as well as mostly gradational changes between divisions. When added together, C1 and C5 have 25–45% clay, 55–70% silt and 5–15% sand; C2 and C4 have 30–50% silt, 25–55% sand and 15–25% clay; and C3 has 25–40% silt, 40–60% sand and minor clay. For the clay fraction and all the separate sand fractions, the carbonate-free percentages are lower than the bulk measurements, indicating removal of very fine carbonate fraction (nannofossils), especially in C1 and C5 divisions, and removal of the coarse carbonate fraction (foraminifera), especially in the C3 division.

The carbonate-free measurements are also similar to those for sequence 11H, and show a distinct grain size oscillation in all divisions that closely tracks that of the bulk grain size.

4.3.4. Grain size statistics

Grain size statistics derived from the analyses of bulk samples are shown in Fig. 12 for both sequences. Mean grain size ranges from very
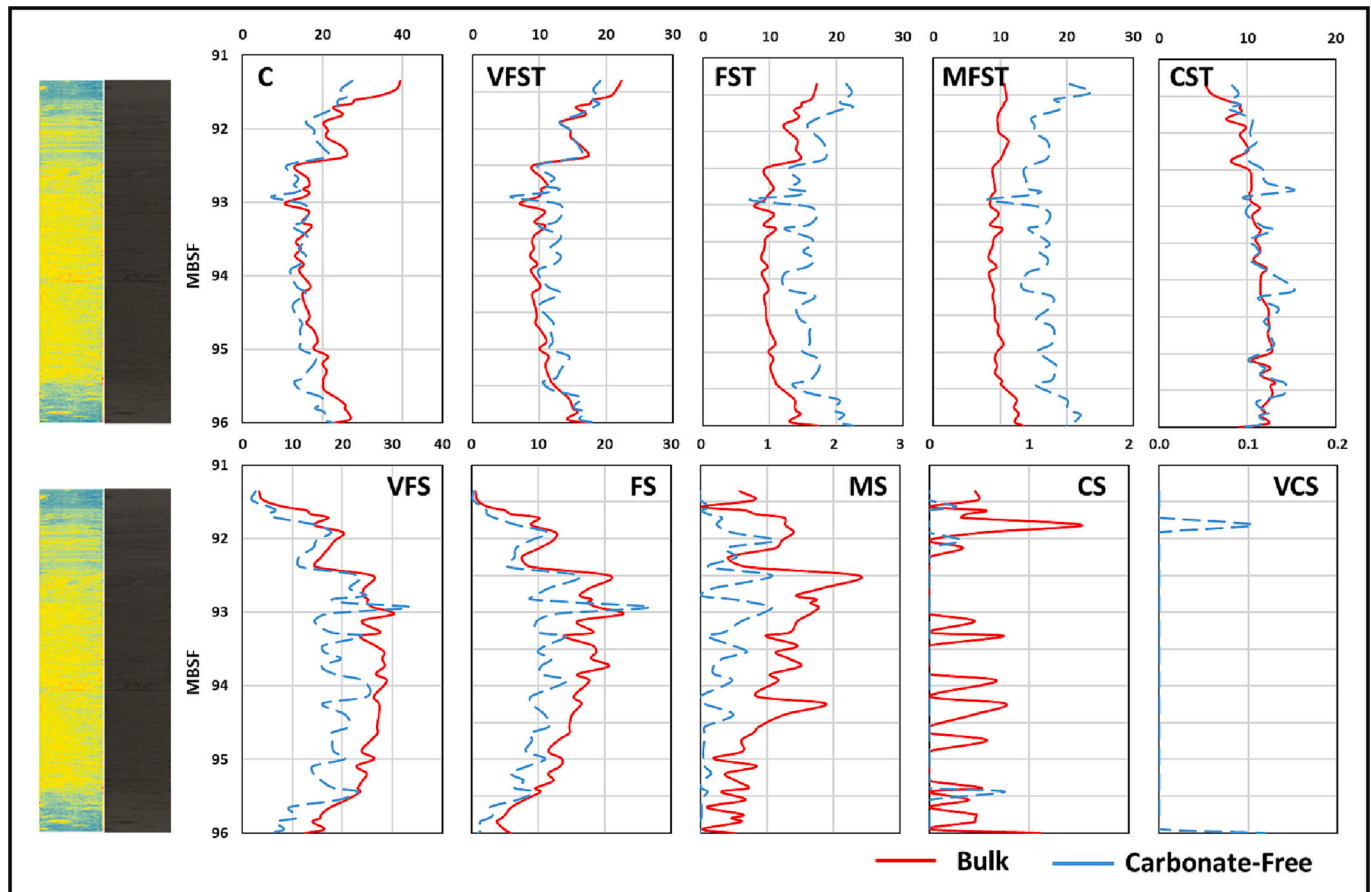

Fig. 8. Relative proportion in percentage (x-axis) of different grain size fractions in sequence 11H. C = clay, VFST = very fine silt, FST = fine silt, MST = medium silt, CST = coarse silt, VFS = very fine sand, FS = fine sand, MS = medium sand, CS = coarse sand, VCS = very coarse sand. Core image is shown to the left of the graph, with false colours (blue = smooth muddy core surfaces, yellow = rough sandy and silty surfaces, red = highly rough surfaces, usually attributed to crack or disturbances). (For interpretation of the references to colour in this figure legend, the reader is referred to the web version of this article.)
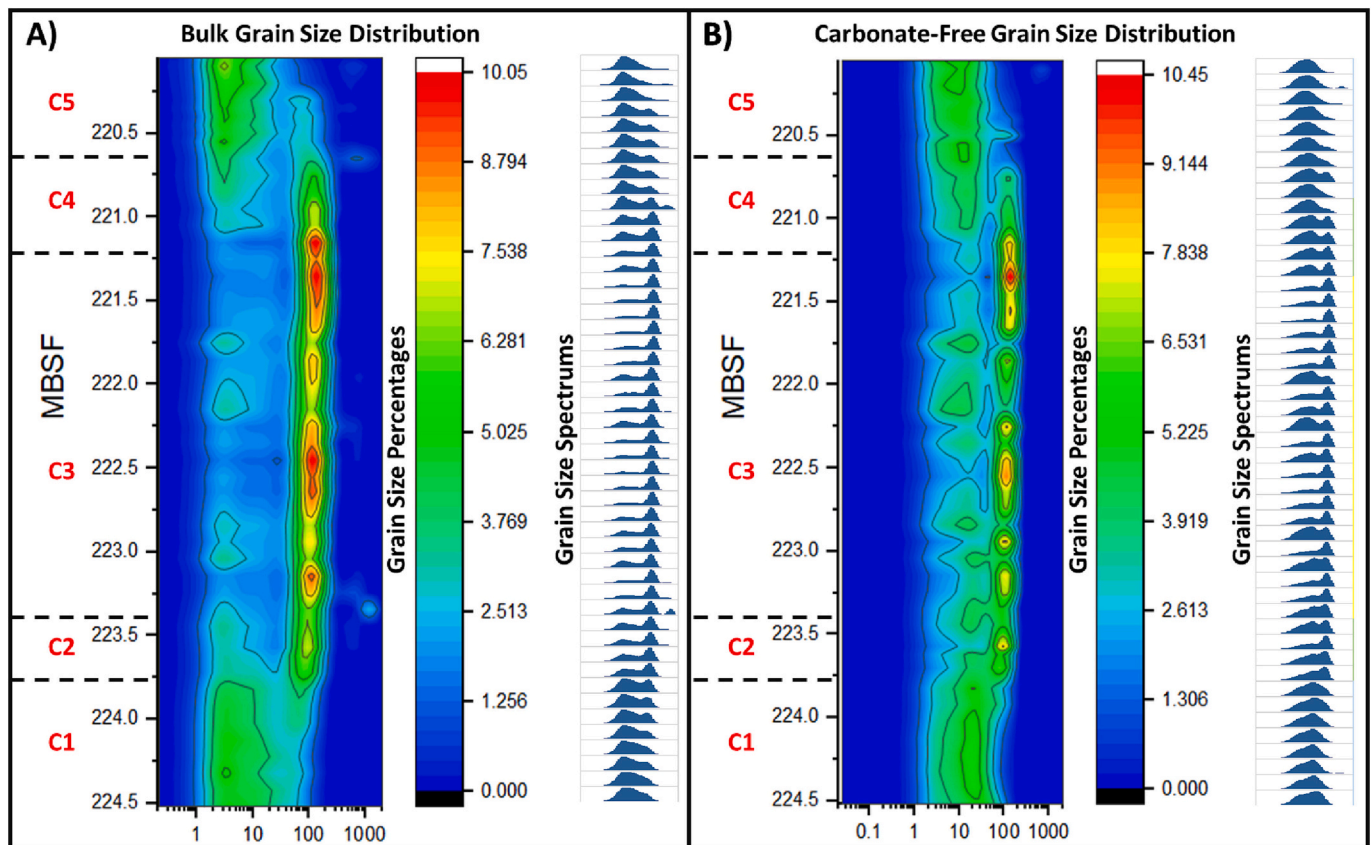
Fig. 9. Heatmap showing relative percentage of grain sizes within Sequence 25X. (A) bulk grain size distribution, and (B) carbonate-free grain size distribution after the removal of carbonate fraction. Grain size distribution spectra are displayed to the right of the heatmaps (blue plots). (For interpretation of the references to colour in this figure legend, the reader is referred to the web version of this article.)

fine silt (7.2 phi, 6.5 μm) to very coarse silt (4.2 phi, 55 μm). When plotted vertically they clearly illustrate the bi-gradational nature of the sequences as well as the abrupt grain size breaks at omission surfaces. The one clear omission surface between C3 and C4 in 11H appears to have cut out the top of C3 and the base of C4 (Fig. 12A). The four omission surfaces in sequence 25X (Fig. 12B) occur at the top at base of C2 and C4 and therefore appear to cut our parts of these divisions. These omission surfaces are marked by abrupt changes in all statistical parameters (Fig. 12C-H).

Both sequences are mostly very poorly sorted throughout, becoming poorly sorted at the top and base only. The skewness varies from coarse to symmetrical in C1 and C5, mainly symmetrical to fine skewed in C2 and C4, and very fine skewed in C3. Kurtosis values are rather varied, mainly within the platykurtic spectrum, but also (in 25X) showing some very platykurtic values in C2, C3 and C4 divisions, and mesokurtic values in C1, C3 and C5 divisions. In general, all statistical parameters indicate an oscillation in grain size properties at the decametric scale.

4.4. Sortable silt and current speed

Sortable silt is taken as the mean size ($\overline{SS}$) of the 10–63 μm fraction of non-carbonate sediment within a sample (McCave et al., 1995b). We have calculated this sortable silt parameter for all grain size analyses through the two sequences and then used it as a proxy for current speed at the time of deposition. Calibration, in this case, follows the method of McCave et al. (2017) for which current speed, U, is given by: $U = 1.31SS - 17.18$ cm s^{-1}.

A comparison of SS% and $\overline{SS}$ for both sequences demonstrates that a close relationship exists between the two values, with a correlation coefficient of 0.877 for 11H and 0.922 for 25X (Fig. 13). This strongly

supports the link between current speed and sediment sorting (Roberts et al., 2017; Culp et al., 2022), and so allows us to infer the likely current speeds for deposition of the two sequences (Fig. 13).

The current speed for sequence 11H ranges between 13.6 cm s^{-1} and 23.6 cm s^{-1}, and for sequence 25X between 11.8 cm s^{-1} and 20.7 cm s^{-1}. As expected, the maximum current speeds in both cases occur within the C3 division and the lowest speeds within C1 and C5 divisions. The grain size oscillation noted in both 11H and 25X sequences can be linked to fluctuation in current speeds of between 1 and 5 cm s^{-1}.

4.5. Sediment composition

4.5.1. Contourite succession

The contourite succession at Site U1389 is characterised by a mixed siliciclastic-biogenic composition (Fig. 14), with a carbonate content between 18 and 45% (Stow et al., 2013; Alsonso et al., 2016). The siliciclastic fraction is dominated by quartz and clay minerals, with minor mica, feldspar (both plagioclase and orthoclase), heavy minerals and volcanic glass, and rare glauconite. The clay mineral fraction includes illite (dominant), kaolinite, chlorite and smectite. Authigenic pyrite, iron mono-sulphides and dolomite are also present in variable amounts (Stow et al., 2013; Alsonso et al., 2016).

The biogenic fraction mainly comprises whole and fragmented calcareous microfossils, especially nannofossils and planktonic foraminifera, but also includes benthic foraminifera and ostracods, and rare siliceous microfossils – sponge spicules, diatoms and radiolaria. Scattered macrofossils occur throughout, mostly fragmented but also found whole. These include gastropods, bivalves, echinoids, cold-water corals and scaphopods. Some proportion of the carbonate fraction (limestone and dolomite) is detrital in origin, derived from erosion of a continental
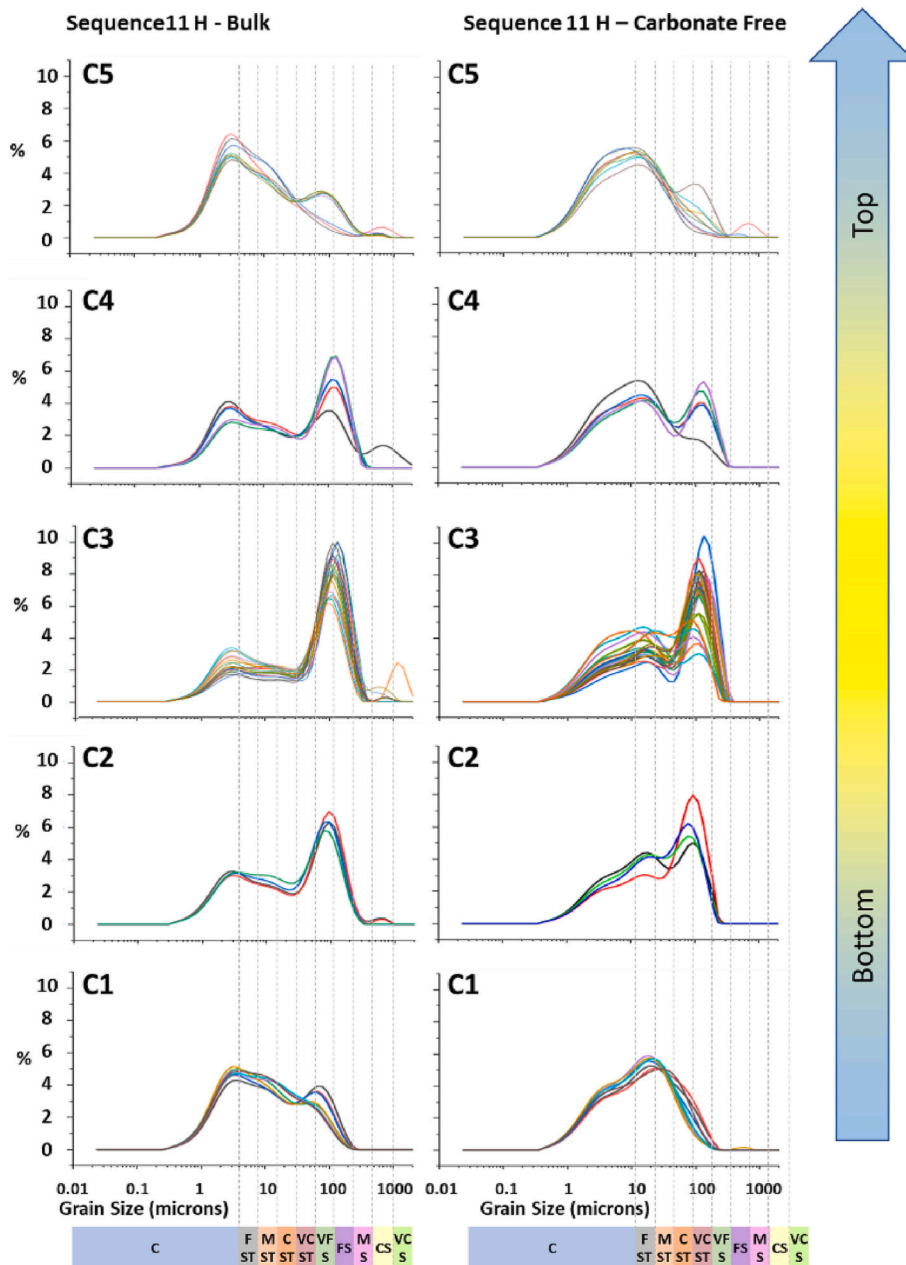
Fig. 10. Grain size distribution spectra of samples taken from the C1 to C5 divisions of sequence 25X.

source. We have not determined the detrital/biogenic ratio for this study, although shipboard estimates suggest a more or less equal proportion of biogenic and detrital carbonate, whereas subsequent laboratory analysis indicates more biogenic calcite than non-biogenic carbonate (mainly dolomite) (Alsonso et al., 2016).

According to shipboard data (Stow et al., 2013), planktonic foraminiferal assemblages through the succession studied herein comprise species representing both cold and warm water. Cold-water species include *Neogloboquadrina pachyderma* (sin) and *Globigerina bulloides*, whereas warm-water species are dominated by *Globigerinoides ruber*, *Globigerinoides trilobus, Globigerinoides sacculifer* and *Sphaeridenellopsis seminulina*. Transitional conditions from temperate to cool subtropical water masses are evidenced by more common *Globorotalia inflata*. The benthic foram assemblage comprises >20 species dominated by *Brizalina, Bulimina, Cassidulina, Melonis*, and *Uvigerina*, with some peaks in *Cibicidoides* and *Trifarina* species.

Our study reveals a dominance of planktic over benthic foram species

throughout, where the planktonic to benthic ratio (P:B) is given by P:B = P/(P + B) * 100%. This mostly ranges from 50 to 75%. There is no systematic trend through the two sequences studied in detail. The ratio of whole to fragmented forams is variable, with broken tests ranging from 30 to 60% of the total.

We show an average bulk sediment composition for contourites at Site U1389 in Fig. 14. One further observation, as noted previously, is the presence of scaphopod horizons (*Arenarias* spp.), with two or more scaphopods in an upright (living) position beneath an inferred omission surface (Fig. 5D).

Organic carbon measurements for Site U1389 reveal a Total Organic Carbon (TOC) content of 0.5% to 1.2% (weight percent) through the contourite succession, and a somewhat irregular variation between these values. The Carbon/Nitrogen (C/N) ratio ranges from 8 to 30 for most of the succession, with one horizon yielding a C/N ratio in excess of 60 (Fig. 15). This ratio is based on C_{org} and the presumption that all the N is also N_{org} although this is simply written as C/N. Most marine C/N
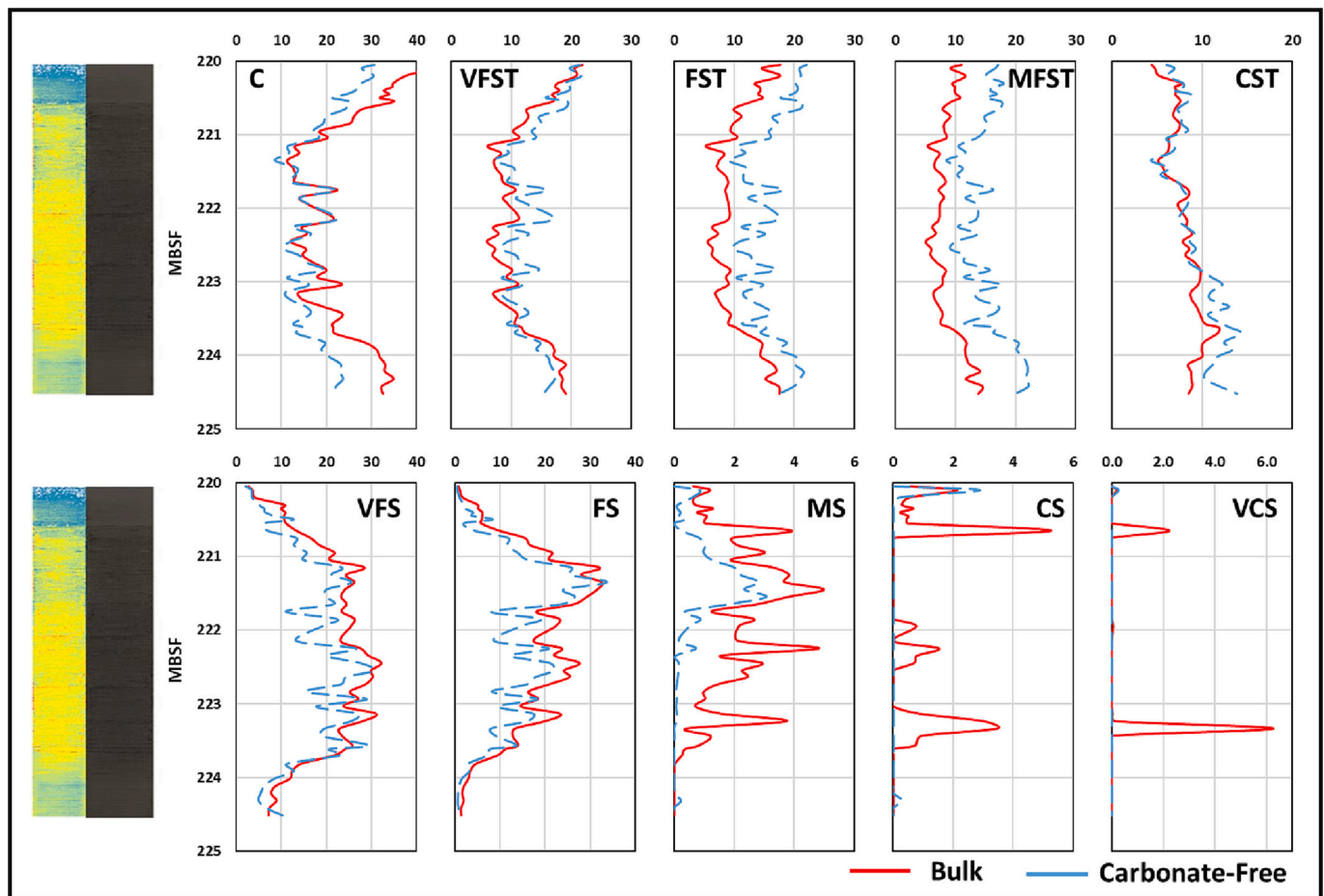
Fig. 11. Relative proportion in percentage (x-axis) of different grain size fractions in sequence 25X. C = clay, VFST = very fine silt, FST = fine silt, MST = medium silt, CST = coarse silt, VFS = very fine sand, FS = fine sand, MS = medium sand, CS = coarse sand, VCS = very coarse sand. Core image is shown to the left of the graph, with false colours (blue = smooth muddy core surfaces, yellow = rough sandy and silty surfaces, red = highly rough surfaces, usually attributed to crack or disturbances). (For interpretation of the references to colour in this figure legend, the reader is referred to the web version of this article.)

ratios are <10 whereas terrestrial values are >18 (approximately), so we have shown a line at C/N = 10 in Fig. 15. Marine organic matter appears to dominate from about 600–350 mbsf, is important from 810 to 600 mbsf, but replaced by more terrestrial organic matter above and below. There is a distinctive spacing between C/N peaks of around 50 m in the section above 350 mbsf, which corresponds to roughly 100 ky. Details of the kerogen composition (organic matter petrology) in the two sequences 11H and 25X is documented below.

4.5.2. Sequence 11H and 25X

Total Organic Carbon (TOC), CaCO$_3$ content and stable isotopes of oxygen and carbon are plotted for each of the two sequences, together with mean grain size for comparison (Fig. 16). The carbon isotopes of the organic matter ($\delta^{13}C_{org}$) and carbonates ($\delta^{13}C_{carb}$) are provided.

CaCO$_3$ content varies between 24.3 and 32.6% in sequence 11H and 26.10–34.45% in sequence 25X. In general, CaCO$_3$ content shows an increase with grain size, being greater in the sandy divisions (C3) compared to the muddy divisions (C1 and C5). This pattern is well developed in 25X but deviates near the base of sequence 11H.

By contrast, TOC and $\delta^{13}C_{org}$ mostly increase in the muddy divisions (C1 and C5) of both sequences. In sequence 11H, TOC varies between 0.26 and 0.51%, and in 25X between 0.17 and 0.56%, with the highest values recorded in the muddy parts of the sequences. The values of $\delta^{13}C_{org}$ (organic matter) show a generally narrow range, between −23.21 and − 24.46 ‰. The $\delta^{13}C_{carb}$ and $\delta^{18}O$ follow a similar pattern to each other that can be correlated to the CaCO$_3$ distribution in both

sequences. The value of $\delta^{13}C_{carb}$ (carbonate) varies between −0.97 and − 1.8 ‰ in sequence 11H and shows a broader range in sequence 25X, varying between −0.62 and + 0.28 ‰. Similarly, the $\delta^{18}O$ shows a broader range in sequence 25X (−0.69 to +0.08 ‰) compared to a range between −0.37 and − 2 ‰ in sequence 11H.

Kerogen composition was examined from sequence 11H only. It ranges from 5 to 100 μm in size, and includes a mixture of marine and terrestrial organic matter (Fig. 17). There appears to be no clear difference in the amount of terrestrial versus marine organic matter in the muddy and sandy divisions. Marine palynomorphs are dominated by dinocysts, zoomorphs (foraminiferal test linings) and acritarchs. The dinocysts are common, moderately well preserved and may represent either autochthonous or reworked material. The zoomorphs are rare and probably the remains of benthic species.

Palynomorphs derived from terrestrial biota are dominated by woody material (phytoclasts) showing various degrees of preservation from degraded and oxidized amorphous organic matter (AOM) to well-preserved organic matter, retaining good vascular cellular structures. Other terrestrial components include freshwater algae and resin, which are quite rare, and amorphous organic matter.

Selected plots for inorganic geochemical ratios are shown in Fig. 18, based on data from de Castro et al. (2020). These relate very closely with the grain size trends. The Zr/Al, Zr/Rb and Si/Al ratios all trend more or less exactly with the mean size, and also show distinct fluctuation in values that match the grain size oscillations observed. The highest values correspond with the sandy division (C3), and the lowest values
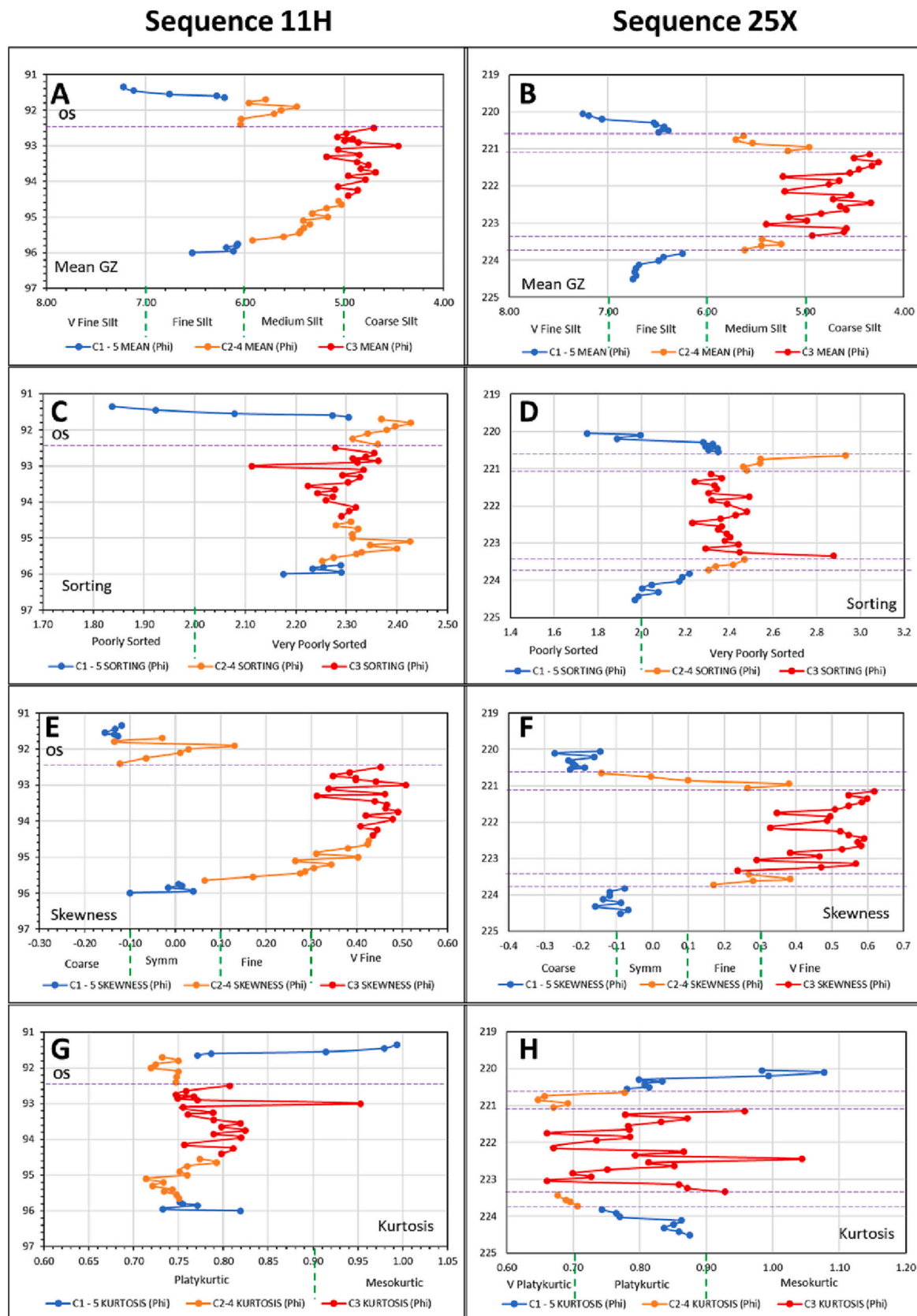
Fig. 12. Grain size statistical parameters plotted with depth through both sequences. A-B Mean Grain Size, C–D Sorting, E-F Skewness, and G-H Kurtosis.
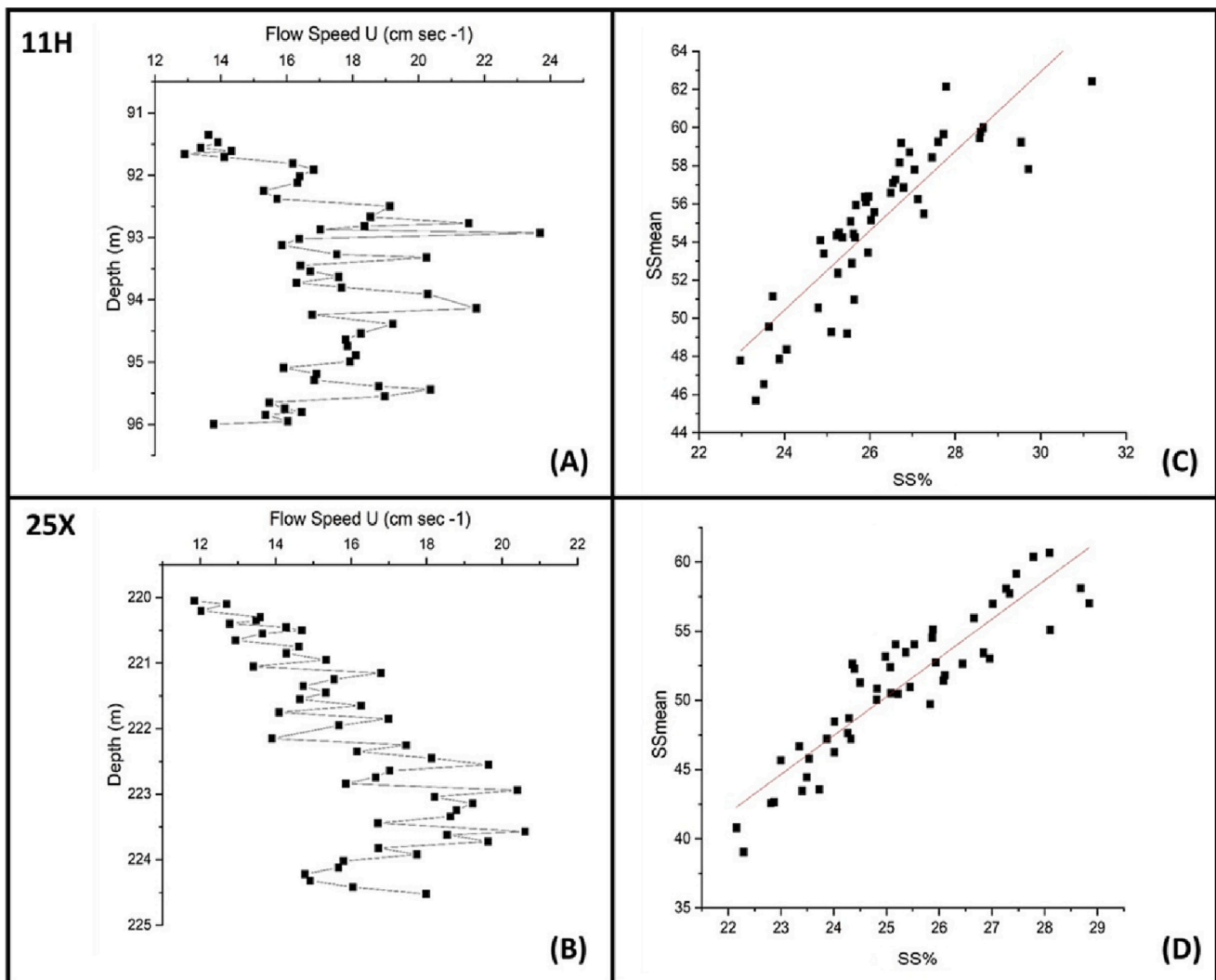
Fig. 13. Sortable silt (SS) data for both sequences: Current speed calculation of the cycle 11H (A) and cycle 25X (B), based on McCave et al. (2017). Cross plots of sortable silt mean and sortable silt percentage of cycle 11H (C) and cycle 25X (D).

with the muddy divisions (C1 and C5). By contrast, the Fe/Ca ratio shows the opposite trend, being highest in the muddy divisions and lowest in the sandy.

5. Discussion

5.1. Contourites, turbidites or hemipelagites?

The results presented here are in line with the interpretation by shipboard scientists (Stow et al., 2013; Hernández-Molina et al., 2016) that the largest part of the Quaternary succession drilled during IODP 339 is of contourite origin. Contourite sedimentation became especially dominant following the regional hiatus at around 2 Ma. The principal reasoning behind this interpretation follows the three-tier approach advocated by many previous studies (Lovell and Stow, 1981; Huneke and Stow, 2008; Stow and Faugères, 2008; Stow et al., 2018):

1. At a *regional scale*, the Expedition 339 sites all lie on a continental margin (water depths 550–1450 m) beneath a known, active bottom current system linked to the Mediterranean Outflow Water. There are regional-wide hiatuses that are noted at most or all the sites drilled. There is a marked shift in mean grain size of the surface sediment from rock outcrop and gravel substrate in the Gibraltar

Gateway, through a broad sand body interpreted as a contourite sheet proximally, to fine muddy mounded and sheeted drifts distally.

2. At a *drift-scale*, the seismic architecture shows sheeted and mounded drifts, elongated in a down-current orientation, together with down-current progradation of seismic units. There are alongslope-oriented channels and moats attributed to bottom-current erosion and floored with sands and sand waves.

3. At the *sediment-scale*, there is indistinct bedding with bi-gradational and mixed sequences, gradational facies boundaries, general lack of primary sedimentary structures apart from some discontinuous lenticular and irregular lamination and rare cross-lamination in sandy facies, pervasive bioturbation with distinct omission surfaces, grain-size oscillation (grading) between fine silty muds and muddy sands, and a very uniform composition throughout of mixed biogenic and terrigenous material.

These three scales of observation combined support a contourite interpretation for most of the post-2 Ma sedimentation at all six sites drilled beneath the Mediterranean Outflow Water. The regional and drift-scale observations are widely supported by much prior work (Hernández-Molina et al., 2006, 2014, 2016; Llave et al., 2006, 2007, 2020). More detailed sediment, paleontological and logging studies also infer contourite deposition for many of the 339 sites (Bahr et al., 2014, 2015; Kaboth et al., 2016; Lofi et al., 2016; Nishida, 2016; Bankole et al.,
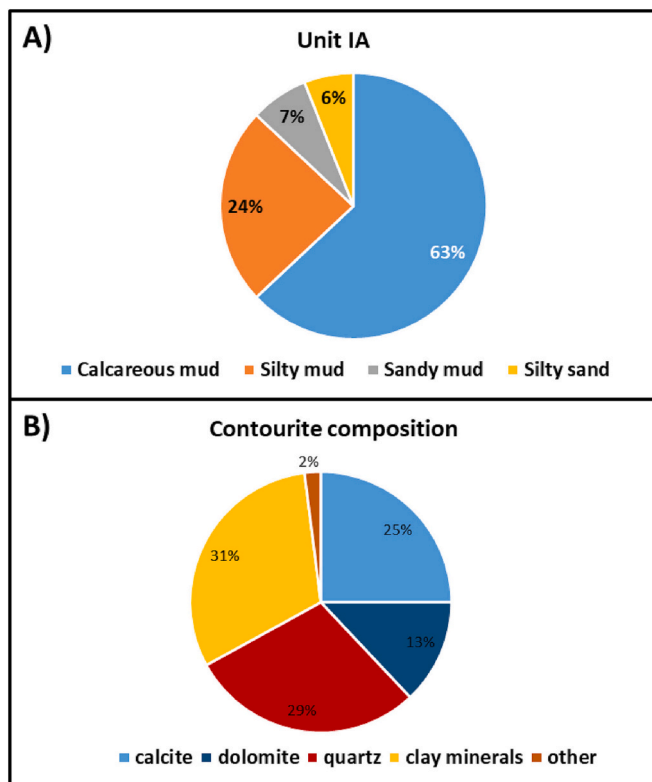
Fig. 14. Sediment composition data for Unit IA based on shipboard data (Stow et al., 2013) and laboratory analyses (Alsonso et al., 2016): (A) Smear slide estimate of textural classes and (B) average composition of contourite sediments.

2020). Grain size characteristics are exactly similar to those documented for contourite sedimentation (Brackenridge et al., 2018; Yu et al., 2020).

Distinction between turbidite and contourite facies in the Gulf of Cadiz has been recently documented by Alsonso et al. (2016) and de Castro et al. (2020). Both indicate that the principal turbidite influx to the region was earlier in the succession – i.e. Pliocene and earliest Pleistocene. In some cases, the turbidites show evidence of reworking by bottom currents. Takashimizu et al. (2016) interpret a series of sandy beds in the deglacial to early Holocene succession at four different sites as sandy contourites. However, they further suggest that these result from the bottom-current reworking of tsunami-emplaced sands. Debrites are also noted in this part of the succession at sites 1386 and 1387 (Stow et al., 2013; Ducassou et al., 2016). In summary, these works all conclude that the middle to late Quaternary succession (as studied here) is dominated by contourites, with some rare examples of bottom-current reworked turbidites or tsunamiites.

In their recent paper focussed on Site U1389 and using Principal Component Analysis of geochemical and sedimentary data, de Castro et al. (2020) interpret a large part (> 50%) of the mud-rich facies as hemipelagite rather than contourite. They point to a slightly different geochemical composition between this facies and the silty contourite facies, the absence of a distinctive ichnofacies or primary sedimentary structures, and the lack of grain-size oscillation bedding (or clear bigradational sequences) as indicative of hemipelagic accumulation.

Whereas we accept that the distinction between hemipelagites and fine muddy contourites deposited under low-energy bottom currents is very difficult, and often impossible, to make, we prefer to interpret the fine muddy facies in this case as muddy contourites (C1 and C5 contourite divisions). This is based on: (a) the probable constant presence of bottom currents linked to the MOW since its onset around 4 Ma, with fluctuation in strength and pathway but no evidence for its complete cessation during deposition of most of the mud-rich facies; (b) the

remarkable uniformity of sediment properties throughout the post-2 Ma Quaternary succession, with no marked changes indicative of a change in depositional process; (c) the absence of a diverse multi-tiered ichnofacies more typical of hemipelagite facies; and (d) the generally high rates of sedimentation (30–40 cm ky^{-1}) throughout, which are considerably higher than for most hemipelagic deposits (Stow and Smillie, 2020).

Furthermore, if we interpret the presence of coarser silty and sandy contourites then we almost certainly have muddy contourites too. If a bottom current is transporting and depositing silt and fine sand then it must also be carrying even more mud (i.e. the finer silts and clays) and depositing this. Interpreting most of the mud (> 50% of the facies according to de Castro et al., 2020) as hemipelagite implies that the bottom current gets turned on and off and, indeed, most of the time it is turned off. We see no clear evidence nor mechanism for this on/off process in the present example.

However, it is true that bottom currents are simply affecting to a greater or lesser extent the sediment that is introduced to them. If the dominant sediment supply is hemipelagic rain from the surface, then the composition of the muddy (C1, C5) contourite will be dominantly hemipelagic in nature. How far the fine biogenic and clay material will be moved laterally by the current is very difficult to ascertain. It may be more accurate to refer to at least some of the muddy facies as a *hybrid contourite-hemipelagite*.

5.2. The bi-gradational sequence

The detailed observations presented here for IODP Site U1389 show approximately 120–130 contourite sequences through the uppermost 1 My of section at each of Holes 1389A and 1389D. The average sequence duration is around 8 ky, but with a wide range (0.4–32 ky) about this mean. Whereas many sequences are bi-gradational, either complete (C1-C2-C3-C4-C5) or mid-cut-out (C1-C2-C4-C5), others are base-cut-out (C3-C2-C1 and C2-C1) or top-cut-out (C1-C2 and C1-C2-C3). These results correspond well with those presented by Pan et al. (in review) for Sites U1386 and U1387, which lie on the Faro Drift some 60 km NW of site 1389, and by de Castro et al. (2020). They provide good validation of the standard bi-gradational facies models for contourites (Stow and Faugères, 2008; Rebesco et al., 2014), noting that the model was developed for *mixed mud-silt* contourites and the sediments studied here are also *mud-rich*. The coarsest parts of some sequences are sandy muds and sandy silts with a coarse silt mean, but very rarely reach a silty sand grade. These relatively coarser parts of the succession show a range of more complex sequence types with several oscillations in grain size and repetition of different C-divisions. These have not previously been recognised in the standard model and its variations, except in the companion paper by Pan et al. (2022), but are clearly an important contourite characteristic. The presence of so many bi-gradational sequences and their systematic variations allows us to refute earlier criticism of the model, notably by Shanmugam (2000, 2006, 2016).

The two sequences selected for detailed study are representative of a complete bi-gradational sequence. They both demonstrate systematic trends in a range of sedimentary features that closely mirror the bi-gradational nature of grain-size properties. These include sedimentary structures (or their absence), bioturbation and ichnofacies, texture and composition. With closely-spaced sampling, two new significant characteristics are observed: (a) the oscillation of grain-size properties over 20–50 cm of section; and (b) the presence of distinct breaks (omission surfaces) in the overall smooth gradational trends. Both of these are best explained by fluctuation in current speed and hence in competence of the bottom current to transport coarser or finer sediment and in its ability to temporarily suspend deposition and/or cause minor erosion at the seafloor.

The oscillation in grain size is mirrored by some of the compositional trends and would seem to reflect fluctuation in current speed. If we assume a constant rate of sedimentation based on shipboard data (Stow
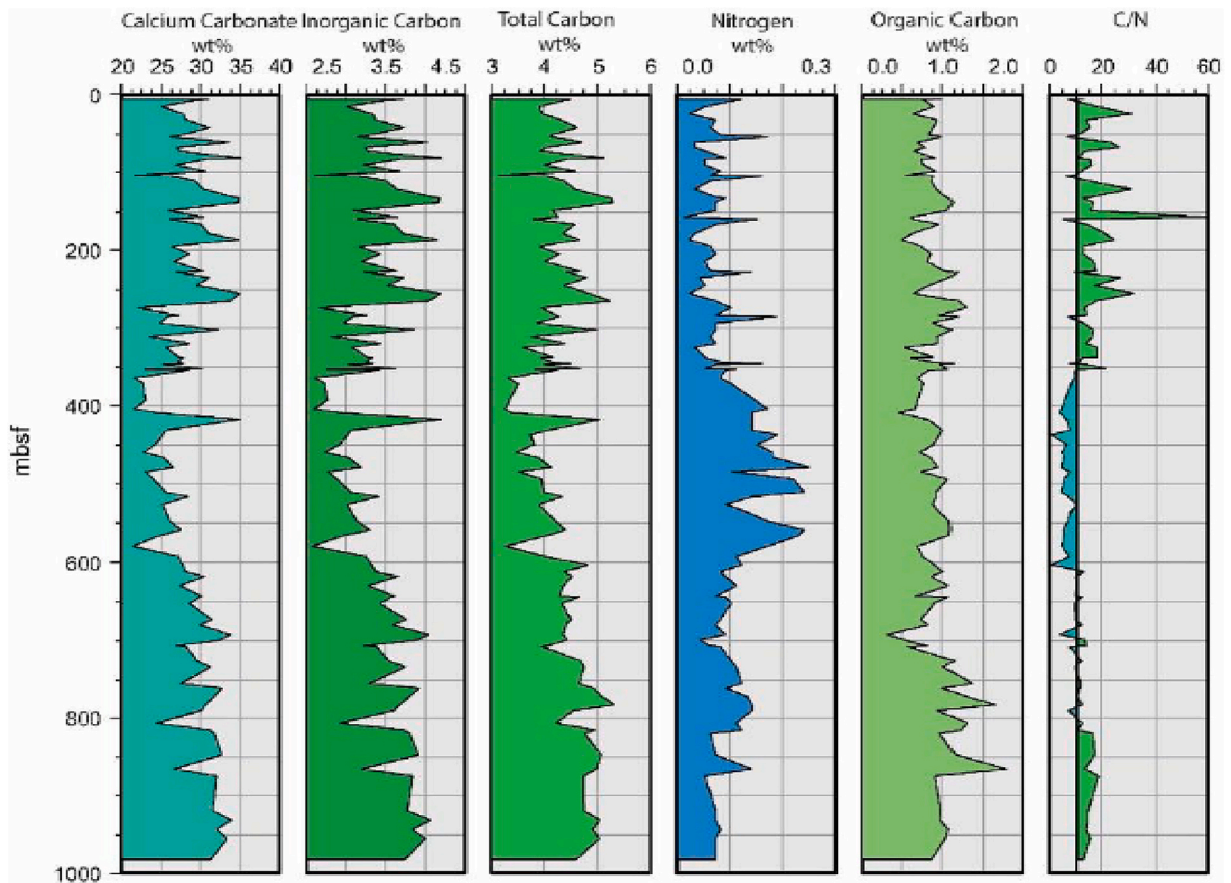
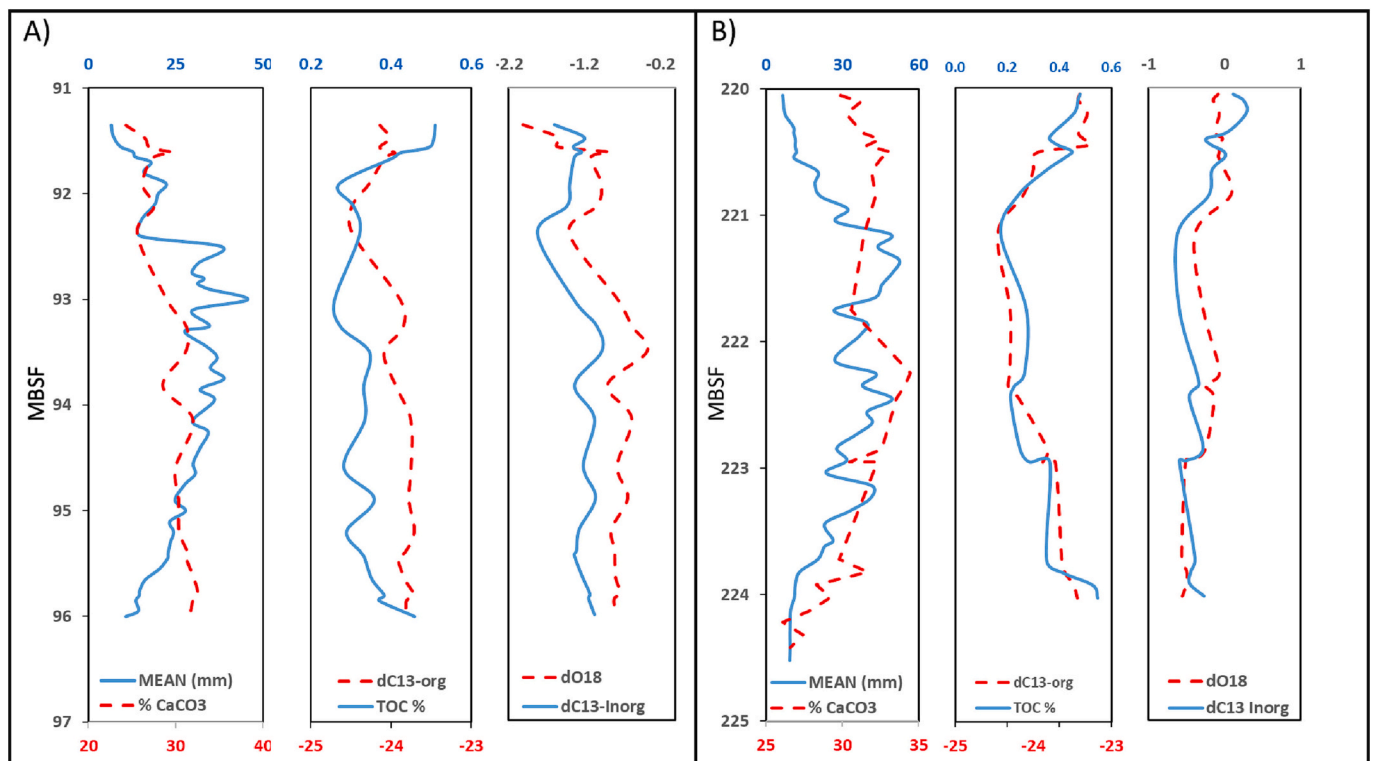**Fig. 15.** Inorganic and organic carbon and nitrogen composition for whole well (data from Stow et al., 2013).

Fig. 16. (A) Distribution of mean grain size, CaCO$_3$, TOC, δ^{13}C$_{org}$ and carbonate oxygen and carbon isotopes through sequence 11H. (B) Distribution of mean grain size, CaCO$_3$, TOC, C13-org and inorganic oxygen and carbon isotopes through sequence 25X.
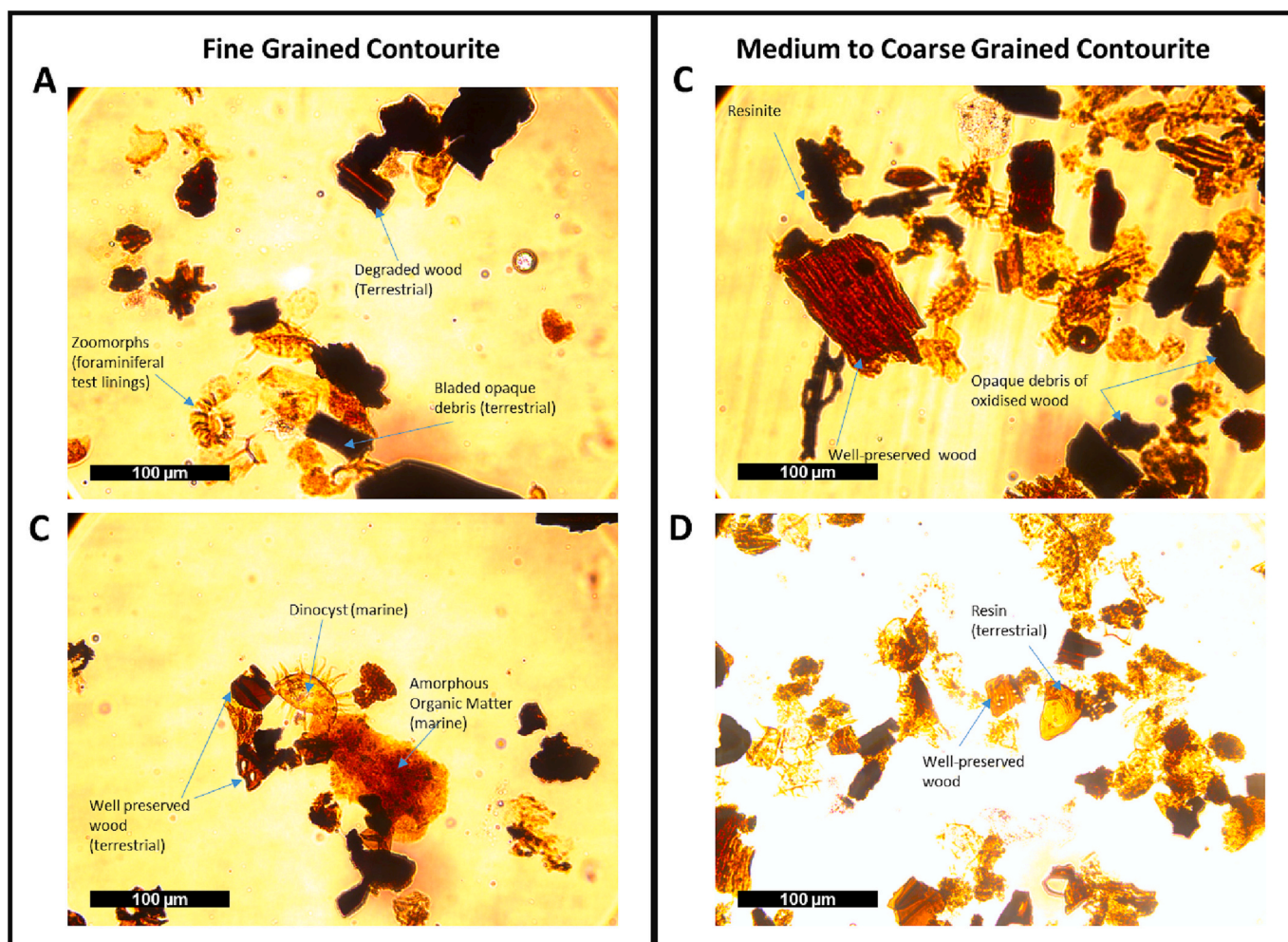
Fig. 17. Kerogen composition of the contourite sediments at site 1389: Palynomorphs in fine grained sediment (A, B) and medium-coarse sediments (C, D).

et al., 2013), then this fluctuation is at around 1 ky intervals, although with a range between 0.5 and 2.0 ky. This sort of fluctuation might be due to changes in the speed of the whole bottom current or, perhaps more likely, the result of mesoscale eddying and anastomosing of the current core(s).

The omission surfaces are more common in the silty/sandy divisions and in the relatively sandier 25× sequence. A first attempt to reconstruct a smooth bi-gradational sequence for 25× from the existing one, extrapolating across inferred breaks due to omission surfaces, suggests that there might be as much as 2–2.5 m of section missing within the 5 m thick sequence (Fig. 20). Using an average rate of deposition for this part of Site U1389 (shipboard data, Stow et al., 2013) gives a 4.5–5.0 ky hiatus within a 15 ky time interval. We emphasise that this is a first crude estimate of missing section, but it is important to note that this represents a significant proportion (25–35%) of the whole and does not take into account any less visible omission surfaces that reflect shorter hiatuses.

5.3. Controls on sequence formation

According to much previous work, two principal controls are considered as the causal mechanism for bi-gradational contourite sequences: (a) long-term fluctuation in mean flow velocity, and (b) variation in sediment supply, either biogenic from surface productivity or terrigenous (Stow et al., 1986, 2002, 2008; Rebesco et al., 2014; de Castro et al., 2020; Pan et al., in review). The collected data presented herein indicate that a combination of these controls have operated for

Site U1389, and that current velocity fluctuation is the more dominant. This is also the conclusion of Pan et al. (in review) for Sites U1386 and U1387, and of de Castro et al. (2020) for Sites U1388 and U1389.

The features observed in this study that are best explained by fluctuation in velocity, gradually and over a few thousand years, include: (a) gradational boundaries between contourite divisions (Figs. 4, 5); (b) gradational changes in mean grain size and associated textural attributes, associated with more rapid fluctuations (Figs. 6–11); (c) most compositional trends that match (e.g. Zr/Al) or mirror (e.g. Fe/Ca) the grain size trends (Fig. 18); and (d) current indicators, such as sharp lenticularity, rare lamination and omission surfaces, that are more evident in the coarser silt and sandy divisions (Figs. 5, 12). It is well known that flow speed, direction and energy of the bottom currents associated with the MOW are affected by variable overflow through the Gibraltar Gateway as a result of climate, sea-level and tectonics, as well as by meso-scale eddies and vertical turbulence in part due to interaction with seafloor topography and the Coriolis effect. On a shorter timescale, velocity fluctuation is caused by interaction with internal tides and waves, and the periodic occurrence of benthic storms (Ambar and Howe, 1979; Farmer and Armi, 1988; Ambar et al., 1999, 2002; Baringer and Price, 1999; Cabecadas et al., 2002; Hernández-Molina et al., 2016).

Other features align more closely with a sediment supply control. In particular, some compositional trends (e.g. carbonate content and proxies, organic carbon) diverge from the grain-size trends in sequence 11H. There is some evidence that the mud-rich sections show a greater influence of terrestrial-derived material, and that the carbonate content varies in part with a productivity driver (Fig. 17). These observations
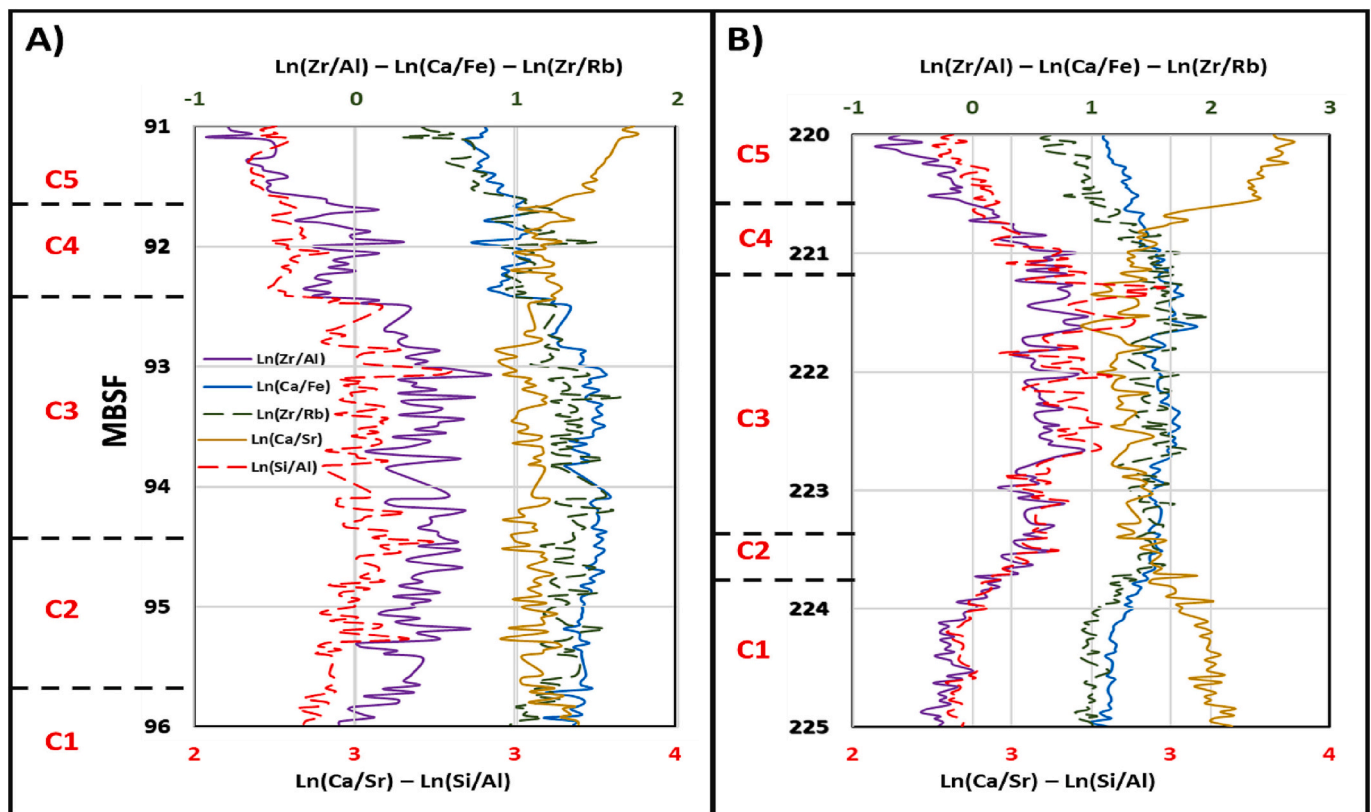
Fig. 18. Ca/Fe, Zr/Al and Ca/Sr ratios of the sequences 11H and 25X, data from (de Castro et al., 2020).

agree with the work of Lofi et al. (2016) on cyclicity across the IODP 339 sites in the Gulf of Cadiz, in which they infer a strong astronomical signature over the past 1.4 My with dominant precession and eccentricity cycles. de Castro et al. (2020) also infer precession-driven changes in Mediterranean hydrography punctuated by millennial-scale variability over the past 250 ky. It seems most likely that this is related to millennial-scale variability of high northern latitude origin – i. e. Dansgaard-Oeschger cycles and Heinrich Events (Bahr et al., 2015; Sierro et al., 2020).

5.4. Sediment provenance and drift budget

The compositional data all support a mixed terrigenous/marine biogenic sediment source, which is typical for many continental slope contourite systems (Hernández-Molina et al., 2008; Stow et al., 2008). The quartz, silicates and clay minerals show a mixed continental signature from mainland Spain (Guadalquivir drainage basin) and the Gibraltar Gateway, perhaps with an additional supply of smectite clays from the mud diapirs and diapiric ridges that lie upstream of Site U1389. These interpretations are in accordance with detailed provenance data given by Alsonso et al. (2016).

The biogenic fraction dominated by nannofossils and planktonic foraminifera indicate a significant pelagic contribution, but much of this is supplied upstream and transported in the bottom current as the $CaCO_3$ content mainly tracks with the grain size. A smaller part of the biogenic fraction is benthic, with whole macrofossils and scaphopods in life position indicative of an in-situ component, whereas fragmented material has been derived from shelf and slope depths and transported alongslope.

The organic matter and organic geochemical signatures confirm an admixture of marine and terrestrial organic carbon. Marine organic matter is most abundant from 600 to 350 mbsf, which equates to about 2.6–1 Ma of the early and mid-Pleistocene, whereas terrestrial organic

matter is most abundant from about 1 Ma. We assume that this latter equates to a greater influx of terrestrial sediment from this time onwards. The marked 100 ky fluctuation in C/N ratio over the past million years is likely due to orbital climate oscillation. However, the relative importance of each source is difficult to ascertain. Terrestrial organic carbon is more susceptible to oxidation and degradation through its transportation towards marine environments, so that which survives this journey is highly refractory and resilient and may therefore constitute a high proportion of carbon in marine sediments (Kumar et al., 2016). Marine organic carbon, by contrast, is much more labile and may suffer significant degradation during transport and reworking in the benthic layer.

Variation of $\delta^{13}C_{org}$ in sediments primarily reflects varying degrees of mixing of terrestrial and marine organic carbon, with their distinct isotopic signatures. $\delta^{13}C_{org}$ values that are derived from terrestrial plants are usually lower than those derived from marine organisms (Mackensen and Bickert, 1999). The $\delta^{13}C$ of plant-derived terrestrial organic carbon range between −30 to −25‰, with an average of −27‰ (Bauer, 2002; Winkelmann and Knies, 2005). Marine-sourced $\delta^{13}C_{org}$, derived from marine phytoplankton, range from −18‰ to −22‰ (Kelleyl et al., 1998; Coffin and Cifuentes, 1999;). The lower $\delta^{13}C_{org}$ values in the fine-grained divisions (C1 and C5) in sequence 25X suggest a greater marine influence than for the coarser divisions (C3). In summary, we interpret these observations as reflecting a higher input of pelagic nannofossil organic matter and relatively less lateral transport, compared with less pelagic input and a greater degree of transport and reworking for the coarser intervals. This relationship holds only partly for sequence 11H, which matches with this sequence being on average finer grained and, hence, being less impacted by lateral transport.

An observed correlation between $\delta^{13}C_{carb}$ and $\delta^{13}C_{org}$ records is generally interpreted as evidence that both the carbonate and organic matter were originally produced in the surface waters of the ocean, and that they have retained their original $\delta^{13}C$ composition (LaPorte et al.,

2009; Korte and Kozur, 2010; Meyer et al., 2013), whereas lack of correlation is interpreted as evidence for diagenetic alteration and/or a mixing of sources (Knoll et al., 1986; Grotzinger et al., 2011; Jiang et al., 2012; Meyer et al., 2013). The data from our two sequences shows relatively poor correlation (Fig. 19), and perhaps indicates significant marine input, but additionally mixed sources as well as degradation and diagenetic effects, especially in the coarser divisions where the permeability is greater. Some support for diagenetic alteration comes from an increase in alkalinity of the interstitial water collected during Expedition 339, especially noted near the sequence 25X (Stow et al., 2013). This may have contributed to changes in the carbon isotope composition in the sediment by leaching of more labile marine organic carbon. It also fits with 25X showing a distinctly poorer correlation (correlation coefficient = 0.374) than 11H (correlation coefficient = 0.693).

The lack of good correlation (positive or negative) between these different geochemical proxies, TOC and $CaCO_3$ content (Fig. 19), and grain size through the two sequences, further suggest the interaction with a larger scale cyclicity, possibly related to glacial-interglacial cycles. This cyclicity of sediment input is clearly noted in the C/N record at Site U1389 (Fig. 15), which shows clear 100 ky cyclicity between more marine and more terrestrial sources of organic matter that correlate negatively with the $CaCO_3$ record. This latter reflects marine planktonic productivity changes coupled with carbonate dilution from terrestrial sediment input.

In summary, these data indicate a mixed sediment provenance for the sheeted drift at Site U1389, as previously inferred for other parts of the Cadiz Contourite Depositional System (Stow et al., 2002; Alsonso et al., 2016; Hernández-Molina et al., 2016), with dominant alongslope transport and minor in-situ diagenetic effects. The sediment budget proposed for the Faro Drift (Bankole et al., 2020), based on data from Sites U1386 and U1387 to the northwest of Site U1389, is 30–35% marine (pelagic biogenic) and 65–70% terrestrial material. They further infer that 90% of the terrigenous material has been transported by alongslope bottom currents, although the actual distance of transport is not determined. Our data for Site U1389 would suggest that the overall drift budget at this location is very similar to that proposed for the Faro Drift.

5.5. Sortable sand and silt: A new approach

The effort to relate grain size of contourites to current speed was initiated by Ledbetter (1986) for the Vema Channel mud and silt contourites in the SW Atlantic. This early work was then refined into the

sortable silt proxy method by (McCave et al., 1995a, 1995b; McCave and Hall, 2006; McCave, 2008), which is much used today (Kleiven et al., 2011; McCave et al., 2017). Sortable silt is taken as the 10–63 μm size fraction, as distinct from the cohesive silt and clay fraction of <10 μm. It refers to only the terrigenous material, having removed biogenic carbonate and opaline silica prior to analysis.

In this paper, we used the relationship between sortable silt mean ($\overline{SS}$) and current speed given by McCave et al. (2017) to infer current speeds between 11.8 cm s^{-1} and 23.6 cm s^{-1} for the two complete sequences analysed in detail (section 4.4 above), as well as fluctuation in current speed of 1–5 cm s^{-1} within each sequence. However, this relationship does not take into account the very fine sand fraction, which appears to be in continuity with the silt fraction from 15 to 150 μm according to extensive grain size data recently published by Brackenridge et al. (2018) and Yu et al. (2020). These data clearly show a systematic contourite depositional trend that extends between about 15–150 μm towards better sorting, and possibly extending to as much as 200 μm (fine sand) for some samples. This trend is most apparent on a mean size/sorting bi-variate plot, and is explained as the result of progressive non-deposition of the fine fraction as current energy (speed) increases.

A similar trend is clearly observed on mean size/skewness and mean size/kurtosis bi-variate plots. The data for Site U1389 (this study) show these same trends (Fig. 21), although most of the sediment mean size is <63 μm in this case, so that we do not see the full range of the trend up to 150 μm. It is worth noting also that Law et al. (2008), using a simplified calculation, state that 16 μm as a minimum size for sortable silt is closest to their observations in a shelf setting, whereas Mehta and Letter (2013) suggest that the boundary between cohesive and non-cohesive silt is around 7.9 μm.

Lamy et al. (2015) also noted the continuity of silt to sand grain size under strong flow of the Antarctic Circumpolar Current through the Drake Passage. Subsequently, Wu et al. (2021) proposed the addition of very fine sand to the sortable silt index, and so use the mean grain size of the sortable silt plus the fine sand fractions (SSFS, 10–125 μm) as a proxy to reconstruct flow speeds of the deep Antarctic Circumpolar Current. Their equation is:

$$U = 0.38\ \overline{SSFS} - 1.77 \text{ cm s}^{-1} \text{ for SSFS in } \mu m$$

Using their equation for our data yields flow speeds of 7.5–21 cm s^{-1} for the sandy C3 divisions, and 4–10.5 cm s^{-1} for the C2 and C4 divisions of both sequences. These values we suggest are a little too low and that we need to develop a bespoke *sortable silt and sand proxy* ($\overline{SSS}$) for the
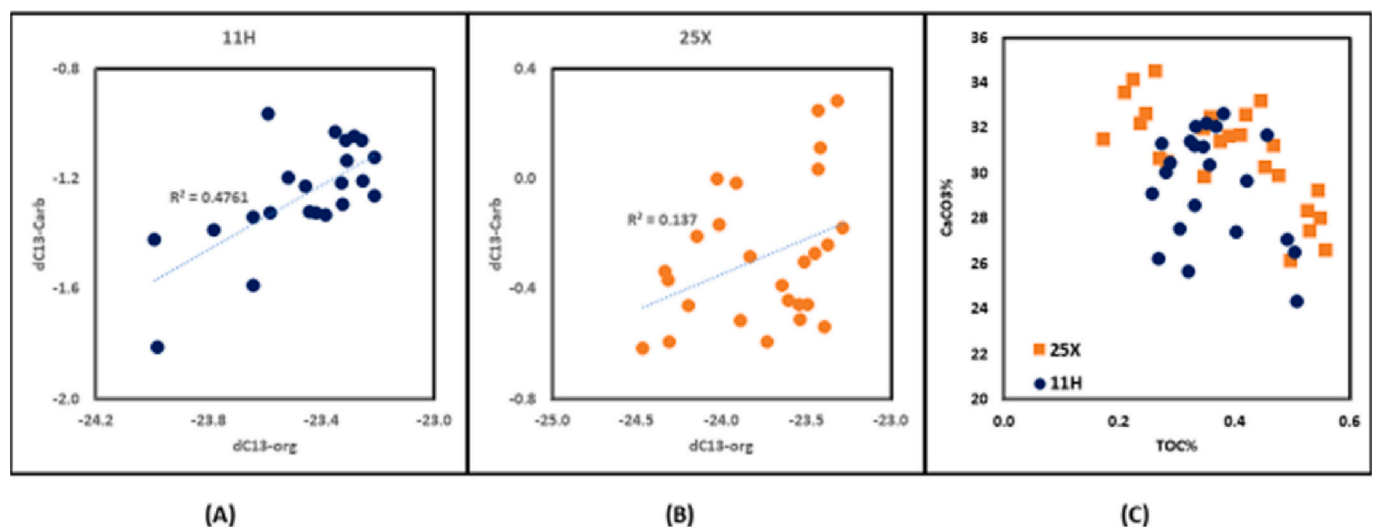

Fig. 19. (A) Relationship between the δ^{13}C$_{org}$ and δ^{13}C$_{carb}$ in sequence 11H. (B) Relationship between the δ^{13}C$_{org}$ and δ^{13}C$_{carb}$ in sequence 25X. (C) Relationship between $CaCO_3$ and TOC% in both sequences.
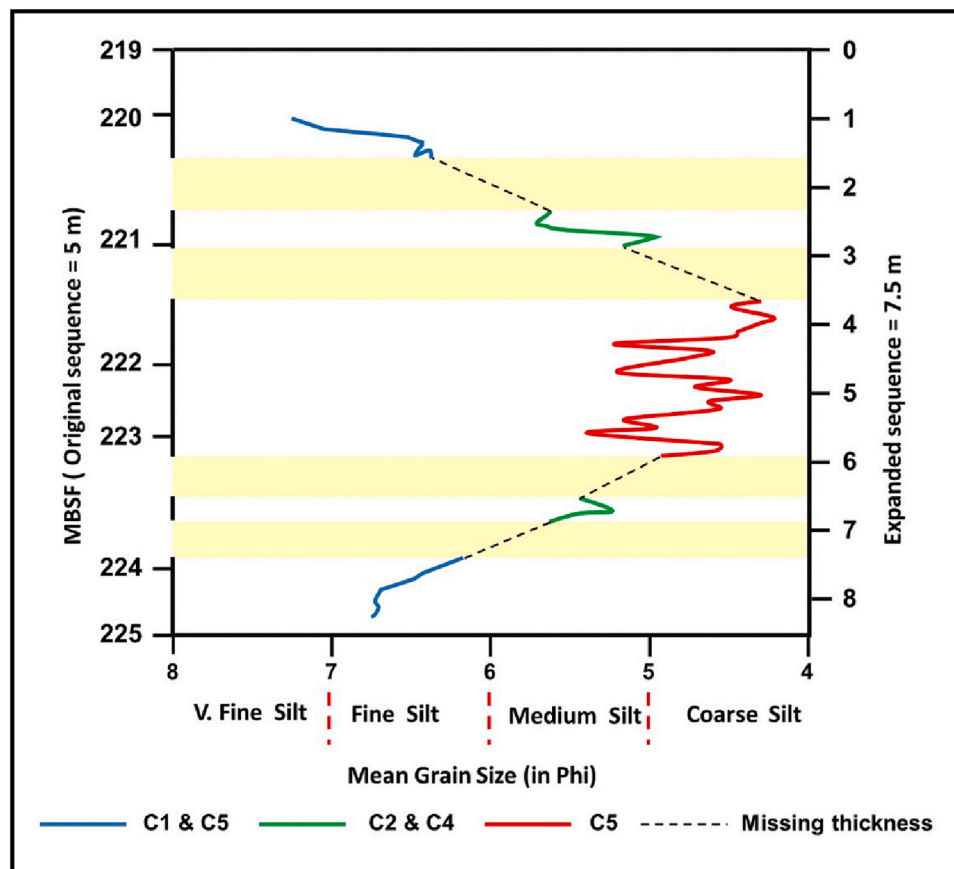
Fig. 20. Reconstruction of a smoothed grain-size profile through bi-gradational sequence 25X. This shows that up to approximately 2.5 m of section is most likely missing across the four omission surfaces identified. The original measured sequence is 5 m thick, whereas the reconstructed sequence is 7.5 m thick.

Cadiz contourites.

We further note that at finer mean grain sizes (i.e. < 15 μm), the cohesive very fine silt and clay material is transported as flocs, whereas at coarser grain sizes (>150 μm), tractional bedload transport becomes more common and coarse lags alternate with deposition from suspension. Recent work (unpublished) shows that flocs and pellets are a primary component of most of the clay and silt grade sediment carried in both bottom currents and hemipelagic transport. Any incorporation of these components into flow speed proxy models will be complex. Clearly there is much work still to be done in developing and refining any new $\overline{SSS}$ or $\overline{SSFS}$ proxy. Grain size analyses carried out for this study used a Laser Malvern Mastersizer, rather than Coulter Counter or Sedigraph as used by McCave et al. (2017), so that further calibration between the different methods is also needed.

6. Conclusion

This paper extends our study of contourite sequences and their geostatistical analysis at Sites U1386 and U1387 (Pan et al., in review) in the Gulf of Cadiz, firstly by documenting the full contourite succession over the past 1.1 My at Site U1389, and secondly by detailed analysis of two selected bi-gradational sequences. This site lies approximately 80 km to the SE of Faro Drift Sites U1386/U1387, closer to the Gibraltar Gateway and hence more proximal to the MOW outflow. Although these proximal regions – the sand sheet and contourite channels – are subject to relatively high bottom current speeds (i.e. > 50 cm s^{-1}), most of the broad sheeted and mounded drifts between channels and in the northern Gulf of Cadiz are swept by lower current speeds. They are made up of mud-rich and mixed mud-sand contourites. Site 1389 is a typical mixed drift system, having mainly clay and silt grade sediment with minor

sand.

The bi-gradational sequence model for contourites is observed throughout. Nearly 300 full and partial sequences are present, with a variable thickness of about 0.13–10.6 m (mean 2.65 m). Partial sequences are common, as are more complex sequences with an irregular repetition of contourite divisions. The average duration of sequences is around 8 ky, but with a wide range of 0.4–32.0 ky. These results are very similar to those reported by Pan et al. (2018, Pan et al., n.d.), and compare well with those of de Castro et al. (2020).

The two sequences studied in detail are both complete bi-gradational sequences showing C1-C5 contourite divisions. Primary sedimentary structures are absent, apart from some bedding-parallel sharp contacts. This is due in part to the fine grain size and cohesive properties of clay and fine silt and in part to subsequent bioturbation. Bioturbation is pervasive and a distinctive pattern of ichnofacies change is observed through each sequence. Textural trends show reverse to normal bi-gradation, which are reflected in compositional trends, with subtle trends in quartz, carbonate, inorganic trace elements, and organic carbon content, as well as in organic matter type. Subtle trends of this kind are useful for recognition of contourites in thick muddy successions with little variation in grain size.

There are abrupt breaks in grain size parameters linked to omission surfaces, especially within the C2-C3-C4 divisions, as well as oscillation in grain size properties typically over 20–50 cm. Both features are significant attributes of contourites and best explained by fluctuations in bottom current speed and/or direction. A first approximation of the amount of section missing due to omission (i.e. non-deposition or erosion) is around 2–2.5 m within a 5 m thick sequence. This suggests around 4.5–5 ky hiatus, and/or extremely condensed section, within a 15 ky time interval, or roughly 25–35% of the time for complete
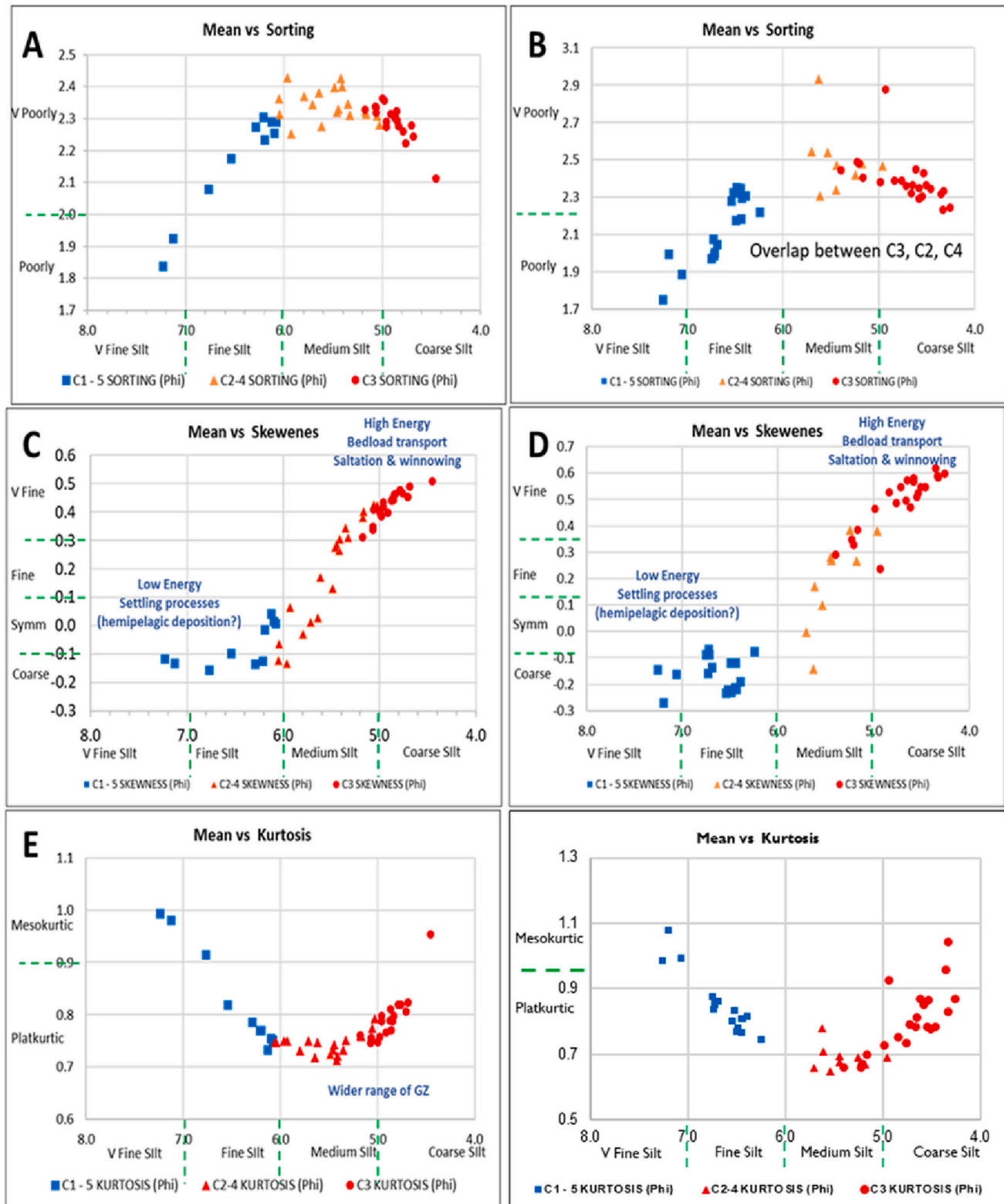
Fig. 21. Bivariate cross plots of grain size statistical parameters for all samples in sequence 11H (left) and 25X (right).

sequence deposition.

The data presented support the conclusion that the bi-gradational contourite sequence and its variations result from the interaction of two principal controls, fluctuation in bottom current velocity and vari-

ation in sediment supply. They further suggest that bottom current velocity is generally the more important. We have estimated the variation in current speed during sequence deposition using the the *sortable silt and fine sand proxy* ($\overline{SSFS}$) proposed by Wu et al. (2021), but that suggest

the values derived are rather too low and that a bespoke *sortable silt and sand proxy* ($\overline{SSS}$) needs to be developed for the Cadiz Contourite Depositional System.

Parts of the overall succession are made up of thick featureless muds with a dominant supply of sediment from a hemipelagic source followed by slow alongslope advection. Such facies can be interpreted as a hybrid contourite-hemipelagite facies. We suggest that this type of hybrid facies is commonplace and is one of the reasons for difficulty in distinguishing fine-grained contourites in both modern and ancient systems.

Data management

The full data for this paper is lodged with the Pangaea website accessible on: https://issues.pangaea.de/browse/PDI-29279

Declaration of Competing Interest

The authors declare that they have no known competing financial interests or personal relationships that could have appeared to influence the work reported in this paper.

Acknowledgements

References

Alsonso, B., Ercilla, G., Casas, D., Stow, D.A.V., Rodríguez-Tovar, F.J., Dorador, J., Hernández-Molina, F.J., 2016. Contourite vs gravity-flow deposits of the Faro Drift (Gulf of Cadiz) during the Pleistocene: sedimentological and mineralogical approaches. Mar. Geol. 377, 77–94. https://doi.org/10.1016/j.margeo.2015.12.016.

Ambar, I., Howe, M., 1979. Observations of the Mediterranean Outflow 1. Mixing in the Mediterranean Outflow. Deep-Sea Res. Part B Oceanogr. Res. Pap. 26, 535–554. https://doi.org/10.1016/0198-0149(79)90095-5.

Ambar, I., Armi, L., Bower, A., Ferreira, T., 1999. Some aspects of time variability of the Mediterranean Water off South Portugal. Deep-Sea Res. Part -Oceanogr. Res. Pap. 46, 1109–1136. https://doi.org/10.1016/S0967-0637(99)00006-0.

Ambar, I., Serra, N., Brogueira, M.J., Cabecadas, G., Abrantes, F., Freitas, P., Goncalves, C., Gonzalez, N., 2002. Physical, chemical and sedimentological aspects of the Mediterranean outflow off Iberia. Deep-Sea Res. Part Ii-Topical Stud. Oceanogr. 49, 4163–4177. https://doi.org/10.1016/S0967-0645(02)00148-0.

Bahr, A., Jiménez-Espejo, F.J., Kolasinac, N., Grunert, P., Hernández-Molina, F.J., Röhl, U., Voelker, A.H.L., Escutia, C., Stow, D.A.V., Hodell, D., Alvarez-Zarikian, C. A., 2014. Deciphering bottom current velocity and paleoclimate signals from contourite deposits in the Gulf of Cádiz during the last 140 kyr: an inorganic geochemical approach. Geochem. Geophys. Geosyst. 15, 3145–3160. https://doi.org/10.1002/2014GC005356.

Bahr, A., Kaboth, S., Jiménez-Espejo, F.J., Sierro, F.J., Voelker, A.H.L., Lourens, L., Röhl, U., Reichart, G.J., Escutia, C., Hernández-Molina, F.J., Pross, J., Friedrich, O., 2015. Persistent monsoonal forcing of Mediterranean Outflow Water dynamics during the late Pleistocene. Geology 43, 951–954. https://doi.org/10.1130/G37013.1.

Bankole, S., Buckman, J., Stow, D., 2020. Unusual components within a fine-grained contourite deposit: significance for interpretation of provenance and the contourite Budget. Minerals 10, 488–498. https://doi.org/10.3390/min10060488.

Baringer, M.O., Price, J.F., 1999. A review of the physical oceanography of the Mediterranean outflow. Mar. Geol. 155, 63–82. https://doi.org/10.1016/S0025-3227(98)00141-8.

Bauer, J.E., 2002. Carbon isotopic composition of DOM. In: In: Biogeochemistry of Marine Dissolved Organic Matter. Elsevier, pp. 405–453. https://doi.org/10.1016/B978-012323841-2/50010-5.

Blott, S.J., Pye, K., 2001. GRADISTAT: a grain size distribution and statistics package for the analysis of unconsolidated sediments. Earth Surf. Process. Landf. 26, 1237–1248. https://doi.org/10.1002/esp.261.

Brackenridge, R.E., Stow, D.A.V., Hernández-Molina, F.J., Jones, C., Mena, A., Alejo, I., Ducassou, E., Llave, E., Ercilla, G., Nombela, M.A., Perez-Arlucea, M., Frances, G.,

2018. Textural characteristics and facies of sand-rich contourite depositional systems. Sedimentology 65, 2223–2252. https://doi.org/10.1111/sed.12463.

Cabecadas, G., Brogueira, M.J., Goncalves, C., 2002. The chemistry of Mediterranean outflow and its interactions with surrounding waters. Deep-Sea Res. Part Ii-Top. Stud. Oceanogr. 49, 4263–4270. https://doi.org/10.1016/S0967-0645(02)00154-6.

Capella, W., Hernández-Molina, F.J., Flecker, R., Hilgen, F.J., Hussain, M., Kouwenhoven, T.J., van Oorschot, M., Sierro, F.J., Stow, D.A.V., Trabucho-Alexandre, J., Tulbure, M.A., de Weger, W., Yousfi, M.Z., Krijgsman, W., 2017. Sandy contourite drift in the late Miocene Rifian Corridor (Morocco): reconstruction of depositional environments in a foreland-basin seaway. Sediment. Geol. 355, 31–57.

Coffin, R.B., Cifuentes, L.A., 1999. Stable isotope analysis of carbon cycling in the Perdido estuary, Florida. Estuaries 22, 917–926. https://doi.org/10.2307/1353071.

Culp, J., Strom, K., Parent, A., Romans, B., 2022. Sorting of fine-grained sediment by currents: Testing the sortable silt hypothesis with laboratory experiments. Sedimentology. https://doi.org/10.1111/SED.12889.

de Castro, S., Hernández-Molina, F.J., de Weger, W., Jiménez-Espejo, F.J., Rodríguez-Tovar, F.J., Mena, A., Llave, E., Sierro, F.J., 2020. Contourite characterization and its discrimination from other deep-water deposits in the Gulf of Cadiz contourite depositional system. Sedimentology 1-41. https://doi.org/10.1111/sed.12813.

Ducassou, E., Fournier, L., Sierro, F.J., Alvarez Zarikian, C.A., Lofi, J., Flores, J.A., Roque, C., 2016. Origin of the large Pliocene and Pleistocene debris flows on the Algarve margin. Mar. Geol. Special Issue 377, 58–76. https://doi.org/10.1016/j.margeo.2015.08.018.

Farmer, D.M., Armi, L., 1988. The flow of Atlantic Water through the Strait of Gibraltar - the flow of Mediterranean Water through the Strait of Gibraltar. Prog. Oceanogr. 21, 1–107. https://doi.org/10.1016/0079-6611(88)90055-9.

Faugères, J.-C., Gonthier, E., Stow, D.A.V., 1984. Contourite drift molded by deep Mediterranean outflow. Geology 12, 296–300. https://doi.org/10.1130/0091-7613(1984)12<296:CDMBDM>2.0.CO;2.

Folk, R.L., Ward, W.C., 1957. Brazos River bar [Texas]; a study in the significance of grain size parameters. J. Sediment. Res. 27, 3–26. https://doi.org/10.1306/74D70646-2B21-11D7-8648000102C1865D.

García, M., Hernández-Molina, F.J., Llave, E., Stow, D.A.V., León, R., Fernández-Puga, M. C., Diaz del Río, V., Somoza, L., 2009. Contourite erosive features caused by the Mediterranean Outflow Water in the Gulf of Cadiz: tectonic and oceanographic Quaternary implications. Mar. Geol. 257, 24–40.

Garcia-Lafuente, J., Delgado, J., Criado-Aldeanueva, F., Bruno, M., del Rio, J., Miguel Vargas, J., 2006. Water mass circulation on the continental shelf of the Gulf of Cadiz. Deep-Sea Res. Part Ii-Top. Stud. Oceanogr. 53, 1182–1197. https://doi.org/10.1016/j.dsr2.2006.04.011.

Gonthier, E.G., Faugères, J.-C., Stow, D.A.V., 1984. Contourite facies of the Faro Drift, Gulf of Cadiz. Geol. Soc. Lond. Spec. Publ. 15, 275–292. https://doi.org/10.1144/GSL.SP.1984.015.01.18.

Grotzinger, J.P., Fike, D.A., Fischer, W.W., 2011. Enigmatic origin of the largest-known carbon isotope excursion in Earth's history. Nat. Geosci. 4, 285–292. https://doi.org/10.1038/ngeo1138.

Hernández-Molina, F.J., Llave, E., Stow, D.A.V., 2008. In: Rebesco, M, Camerlenghi, A (Eds.), Contourites, Developments in Sedimentology Series, 60. Elsevier, pp. 379–400.

Hernández-Molina, F.J., Llave, E., Stow, D.A.V., García, M., Somoza, L., Vázquez, J.T., Lobo, F.J., Maestro, A., Díaz del Río, V., León, R., Medialdea, T., Gardner, J., 2006. The contourite depositional system of the Gulf of Cádiz: a sedimentary model related to the bottom current activity of the Mediterranean outflow water and its interaction with the continental margin. Deep Sea Res. Part II Top. Stud. Oceanogr. 53, 1420–1463. https://doi.org/10.1016/j.dsr2.2006.04.016.

Hernández-Molina, F.J., Llave, E., Preu, B., Ercilla, G., Fontan, A., Bruno, M., Serra, N., Gomiz, J.J., Brackenridge, R.E., Sierro, F.J., Stow, D.A.V., García, M., Juan, C., Sandoval, N., Arnaiz, A., 2014. Contourite processes associated with the Mediterranean Outflow Water after its exit from the Strait of Gibraltar: Global and conceptual implications. Geology 42, 227–230. https://doi.org/10.1130/G35083.1.

Hernández-Molina, F.J., Sierro, F.J., Llave, E., Roque, C., Stow, D.A.V., Williams, T., Lofi, J., Van der Schee, M., Arnáiz, A., Ledesma, S., Rosales, C., Rodríguez-Tovar, F. J., Pardo-Igúzquiza, E., Brackenridge, R.E., 2016. Evolution of the gulf of Cadiz margin and Southwest Portugal contourite depositional system: Tectonic, sedimentary and paleoceanographic implications from IODP expedition 339. Mar. Geol. 377, 7–39. https://doi.org/10.1016/j.margeo.2015.09.013.

Hollister, C.D., 1993. The concept of deep-sea contourites. Sediment. Geol. 82, 5–11. https://doi.org/10.1016/0037-0738(93)90109-I.

Hollister, C.D., Heezen, B.C., 1972. The geologic effects of ocean bottom currents: Western North Atlantic. In: Gordon, A.L. (Ed.), Studies in Physical Oceanography, vol. v. 2. Gordon & Breach, New York.

Howe, M., 1982. The Mediterranean Water Outflow in the Gulf of Cadiz. Oceanogr. Mar. Biol. 20, 37–64.

Huneke, H., Stow, D.A.V., 2008. Identification of ancient contourites: Problems and paleoceanographic significance. In: Rebesco, M., Camerlenghi, A. (Eds.), Developments in Sedimentology. Elsevier, Contourites, pp. 323–344. https://doi.org/10.1016/S0070-4571(08)10017-6.

Jiang, G., Wang, X., Shi, X., Xiao, S., Zhang, S., Dong, J., 2012. The origin of decoupled carbonate and organic carbon isotope signatures in the early Cambrian (ca. 542–520Ma) Yangtze platform. Earth Planet. Sci. Lett. 317–318, 96–110. https://doi.org/10.1016/j.epsl.2011.11.018.

Kaboth, S., Bahr, A., Reichart, G.-J., Jacobs, B., Lourens, L.J., 2016. New insights into upper MOW variability over the last 150kyr from IODP 339 Site U1386 in the Gulf of Cadiz. Mar. Geol. 377, 136–145. https://doi.org/10.1016/j.margeo.2015.08.014.

Kelleyl, C.A., Coffin, R.B., Cifuentes, L.A., 1998. Stable isotope evidence for alternative bacterial carbon sources in the Gulf of Mexico. Limnol. Oceanogr. 43, 1962–1969. https://doi.org/10.4319/lo.1998.43.8.1962.

Kleiven, H.F., Hall, I.R., McCave, I.N., Knorr, G., Jansen, E., 2011. Deep-water formation and climate change in the North Atlantic during the Mid-Pleistocene. Geology 39, 343–346.

Knoll, A.H., Hayes, J.M., Kaufman, A.J., Swett, K., Lambert, I.B., 1986. Secular variation in carbon isotope ratios from Upper Proterozoic successions of Svalbard and East Greenland. Nature 321, 832–838. https://doi.org/10.1038/321832a0.

Korte, C., Kozur, H.W., 2010. Carbon-isotope stratigraphy across the Permian–Triassic boundary: a review. J. Asian Earth Sci. 39, 215–235. https://doi.org/10.1016/j.jseaes.2010.01.005.

Kumar, V., Tiwari, M., Nagoji, S., Tripathi, S., 2016. Evidence of anomalously Low δ 13 C of marine organic matter in an Arctic fjord. Sci. Rep. 6, 36192. https://doi.org/10.1038/srep36192.

Lamy, F., et al., 2015. Glacial reduction and millennial-scale variations in Drake Passage throughflow. Proc. Natl. Acad. Sci. USA112, 13496–13501. https://doi.org/10.1073/pnas.1509203112.

LaPorte, D.F., Holmden, C., Patterson, W.P., Loxton, J.D., Melchin, M.J., Mitchell, C.E., Finney, S.C., Sheets, H.D., 2009. Local and global perspectives on carbon and nitrogen cycling during the Hirnantian glaciation. Palaeogeogr. Palaeoclimatol. Palaeoecol. 276, 182–195. https://doi.org/10.1016/j.palaeo.2009.03.009.

Law, B.A., Hill, P.S., Milligan, T.G., Curran, K.J., Wiberg, P.L., Wheatcroft, R.A., 2008. Size sorting of fine-grained sediments during erosion: results from western Gulf of Lions. Cont. Shelf Res. 28, 1935–1946.

Ledbetter, M.T., 1986. A late Pleistocene time-series of bottom-current speed in the Vema Channel. Palaeogeogr. Palaeoclimatol. Palaeoecol. 53, 97–105. https://doi.org/10.1016/0031-0182(86)90040-4.

Llave, E., Schönfeld, J., Hernández-Molina, F.J., Mulder, T., Somoza, L., Díaz del Río, V., Sánchez-Almazo, I., 2006. High-resolution stratigraphy of the Mediterranean outflow contourite system in the Gulf of Cadiz during the late Pleistocene: the impact of Heinrich events. Mar. Geol. 227, 241–262. https://doi.org/10.1016/j.margeo.2005.11.015.

Llave, E., Hernández-Molina, F.J., Somoza, L., Stow, D.A.V., Río, V.D.D., 2007. Quaternary evolution of the contourite depositional system in the Gulf of Cadiz. Geol. Soc. Lond. Spec. Publ. 276, 49–79. https://doi.org/10.1144/GSL.SP.2007.276.01.03.

Llave, E., Hernández-Molina, F.J., García, M., Ercilla, G., Roque, C., Juan, C., Mena, A., Preu, B., Van Rooij, D., Rebesco, M., Brackenridge, R., Jané, G., Gómez-Ballesteros, M., Stow, D., 2020. Contourites along the Iberian continental margins: conceptual and economic implications. Geol. Soc. Lond. Spec. Publ. 476, 403–436. https://doi.org/10.1144/SP476-2017-46.

Lobo, F.J., Hernández-Molina, F.J., Somoza, L., Rodero, J., Maldonado, A., Barnolas, A., 2000. Patterns of bottom current flow deduced from dune asymmetries over the Gulf of Cadiz shelf (Southwest Spain). Mar. Geol. 164, 91–117. https://doi.org/10.1016/S0025-3227(99)00132-2.

Lofi, J., Voelker, A.H.L., Ducassou, E., Hernández-Molina, F.J., Sierro, F.J., Bahr, A., Galvani, A., Lourens, L.J., Pardo-Igúzquiza, E., Pezard, P., Rodríguez-Tovar, F.J., Williams, T., 2016. Quaternary chronostratigraphic framework and sedimentary processes for the Gulf of Cadiz and Portuguese Contourite Depositional Systems derived from natural Gamma Ray records. Mar. Geol. Spec. Issue 377, 40–57. https://doi.org/10.1016/j.margeo.2015.12.005.

Lovell, J.P.B., Stow, D.A.V., 1981. Identification of Ancient Sandy Contourites. Geology 9, 347–349.

Mackensen, A., Bickert, T., 1999. Stable Carbon Isotopes in Benthic Foraminifera: Proxies for deep and bottom water circulation and new production. In: Fischer, G., Wefer, G. (Eds.), Use of Proxies in Paleoceanography: Examples from the South Atlantic. Springer, Berlin, Heidelberg, pp. 229–254. https://doi.org/10.1007/978-3-642-58646-0_9.

McCave, I.N., 2008. Size sorting during transport and deposition of fine sediments. In: Rebesco, M., Camerlenghi, A. (Eds.), Developments in Sedimentology. Elsevier, Contourites, pp. 121–142.

McCave, I.N., Hall, I.R., 2006. Size sorting in marine muds: Processes, pitfalls, and prospects for paleoflow-speed proxies. Geochem. Geophys. Geosyst. 7, Q10N05. https://doi.org/10.1029/2006GC001284.

McCave, I.N., Manighetti, B., Beveridge, N.A.S., 1995a. Circulation in the glacial North Atlantic inferred from grain-size measurements. Nature 374, 149–152. https://doi.org/10.1038/374149a0.

McCave, I.N., Manighetti, B., Robinson, S.G., 1995b. Sortable silt and fine sediment size/composition slicing: Parameters for palaeocurrent speed and palaeoceanography. Paleoceanography 10, 593–610. https://doi.org/10.1029/94PA03039.

McCave, I.N., Thornalley, D.J.R., Hall, I.R., 2017. Relation of sortable silt grain-size to deep-sea current speeds: Calibration of the 'Mud Current Meter.'. Deep Sea Res. Part Oceanogr. Res. Pap. 127, 1–12. https://doi.org/10.1016/j.dsr.2017.07.003.

Medialdea, T., Somoza, L., Pinheiro, L.M., Fernández-Puga, M.C., Vázquez, J.T., León, R., Ivanov, M.K., Magalhaes, V., Díaz-del-Río, V., Vegas, R., 2009. Tectonics and mud volcano development in the Gulf of Cádiz. Mar. Geol. Spec. Issue 261, 48–63. https://doi.org/10.1016/j.margeo.2008.10.007.

Mehta, A.J., Letter, J.V., 2013. Comments on the transition between cohesive and cohesionless sediment bed exchange. Estuar. Coast. Shelf Sci. 131, 319–324.

Meyer, K.M., Yu, M., Lehrmann, D., van de Schootbrugge, B., Payne, J.L., 2013. Constraints on early Triassic carbon cycle dynamics from paired organic and inorganic carbon isotope records. Earth Planet. Sci. Lett. 361, 429–435. https://doi.org/10.1016/j.epsl.2012.10.035.

Mulder, T., Voisset, M., Lecroart, P., Le Drezen, E., Gonthier, E., Hanquiez, V., Faugeres, J.C., Habgood, E., Hernandez-Molina, F.J., Estrada, F., Llave-Barranco, E.,

Poirier, D., Gorini, C., Fuchey, Y., Voelker, A., Freitas, P., Sanchez, F.L., Fernandez, L.M., Kenyon, N.H., Morel, J., 2003. The Gulf of Cadiz: an unstable giant contouritic levee. Geo-Mar. Lett. 23, 7–18. https://doi.org/10.1007/s00367-003-0119-0.

Nishida, N., 2016. Microstructure of muddy contourites from the Gulf of Cádiz. Mar. Geol. Special Issue 377, 110–117. https://doi.org/10.1016/j.margeo.2015.08.017.

Pan, J., Stow, D., Smillie, Z., Burgess, P., n.d. The bi-gradational contourite sequence: a geostatistical approach. Deep-Sea Res. I., (in press).

Rebesco, M., Hernández-Molina, F.J., Van Rooij, D., Wåhlin, A., 2014. Contourites and associated sediments controlled by deep-water circulation processes: State-of-the-art and future considerations. Mar. Geol. 352, 111–154. https://doi.org/10.1016/j.margeo.2014.03.011, 50th Anniversary Special Issue.

Roberts, J., McCave, I.N., McClymont, E.L., Kender, S., Hillenbrand, C.-D., Matano, R., Hodell, D.A., Peck, V.L., 2017. Deglacial changes in flow and frontal structure through the Drake Passage. Earth Planet. Sci. Lett. 474, 397–408. https://doi.org/10.1016/j.epsl.2017.07.004.

Rogerson, M., Rohling, E.J., Weaver, P.P.E., Murray, J.W., 2005. Glacial to interglacial changes in the settling depth of the Mediterranean Outflow plume. Paleoceanography 20, PA3007. https://doi.org/10.1029/2004PA001106.

Rosenbaum, G., Lister, G.S., Duboz, C., 2002. Relative motions of Africa, Iberia and Europe during Alpine orogeny. Tectonophysics 359, 117–129. https://doi.org/10.1016/S0040-1951(02)00442-0.

Shanmugam, G., 2000. 50 years of the turbidite paradigm (1950s—1990s): deep-water processes and facies models—a critical perspective. Mar. Pet. Geol. 17, 285–342.

Shanmugam, G., 2006. Deep-Water Bottom Currents. Handbook of Petroleum Exploration and Production. Elsevier, pp. 85–139.

Shanmugam, G., 2016. The Contourite Problem. In: Mazumder, R. (Ed.), Sediment Provenance. Elsevier.

Sierro, F.J., Hodell, D.A., Andersen, N., Azibeiro, L.A., Jimenez-Espejo, F.J., Bahr, A., Flores, J.A., Ausin, B., Rogerson, M., Lozano-Luz, R., 2020. Mediterranean Overflow over the last 250 kyr: Freshwater forcing from the tropics to the ice sheets. Paleoceanogr. Paleoclimatol. 35, e2020PA003931.

Stow, D.A.V., 1977. Late Quaternary Stratigraphy and Sedimentation on the Nova Scotian Outer Continental Margin. Unpublished PhD thesis,. Dalhousie University, Canada, p. 360.

Stow, D.A.V., 1979. Distinguishing between fine-grained turbidites and contourites on the Nova Scotian deep. Water Margin. Sedimentol. 26, 371–387.

Stow, D.A.V., 1982. Bottom currents and contourites in the North Atlantic. Bull. Inst. Geol. Bassin d'Aquitaine 31, 151–166.

Stow, D.A.V., 2005. Sedimentary Rocks in the Field: A Colour Guide. Manson Publishing, p. 320.

Stow, D.A.V., Faugères, J.-C., 2008. Contourite facies and the facies model. In: Rebesco, M., Camerlenghi, A. (Eds.), Developments in Sedimentology. Elsevier, Contourites, pp. 223–256. https://doi.org/10.1016/S0070-4571(08)10013-9.

Stow, D.A.V., Lovell, J.P.B., 1979. Contourites: their recognition in modern and ancient sediments. Earth Sci. Rev. 14, 251–291.

Stow, D.A.V., Piper, D.J.W., 1984. Deep-water fine-grained sediments: facies models. Geol. Soc. Lond. Spec. Publ. 15, 611–646. https://doi.org/10.1144/GSL.SP.1984.015.01.38.

Stow, D., Smillie, Z., 2020. Distinguishing between deep-water sediment facies: turbidites, contourites and hemipelagites. Geosciences 10, 68. https://doi.org/10.3390/geosciences10020068.

Stow, D.A.V., Faugères, J.-C., Gonthier, E., 1986. Facies distribution and textural variation in Faro Drift contourites: Velocity fluctuation and drift growth. Mar. Geol. 72, 71–100.

Stow, D.A.V., Faugères, J.-C., Howe, J.A., Pudsey, C.J., Viana, A.R., 2002. Bottom currents, contourites and deep-sea sediment drifts: current state-of-the-art. Geol. Soc. Lond. Mem. 22, 7–20. https://doi.org/10.1144/GSL.MEM.2002.022.01.02.

Stow, D.A.V., Hunter, S., Wilkinson, D., Hernández-Molina, F.J., 2008. The nature of contourite deposition. In: Rebesco, M., Camerlenghi, A. (Eds.), Contourites, Developments in Sedimentology 60. Elsevier, pp. 143–156.

Stow, D.A.V., Hernández-Molina, F.J., Alvarez Zarikian, C.A., Expedition 339 Scientists, 2013. Expedition 339 summary. In: Proceedings of the Integrated Ocean Drilling Program, p. 339. https://doi.org/10.2204/iodp.proc.339.2013.

Stow, D., Smillie, Z., Pan, J., Esentia, I.P., 2018. Deep-sea contourites: Sediments and cycles. In: Cochran, J. Kirk, Bokuniewicz, J. Henry, Yager, L. Patricia (Eds.), Encyclopedia of Ocean Sciences, , 3rd editionvol. 4. Elsevier, pp. 111–120. https://doi.org/10.1016/B978-0-12-409548-9.10879-6.

Takashimizu, Y., Kawamura, R., Rodríguez-Tovar, F.J., Dorador, J., Ducassou, E., Hernández-Molina, F.J., Stow, D.A.V., Alvarez-Zarikian, C.A., 2016. Reworked tsunami deposits by bottom currents: Circumstantial evidences from late Pleistocene to early Holocene in the Gulf of Cádiz. Mar. Geol., Special Issue 377, 95–109. https://doi.org/10.1016/j.margeo.2015.09.009.

Winkelmann, D., Knies, J., 2005. Recent distribution and accumulation of organic carbon on the continental margin west off Spitsbergen. Geochem. Geophys. Geosyst. 6 https://doi.org/10.1029/2005GC000916.

Wu, S., et al., 2021. Orbital- and millennial-scale Antarctic Circumpolar current variability in Drake Passage over the past 140,000 years. Nat. Commun. https://doi.org/10.1038/s41467-021-24264-9.

Yu, X., Stow, D., Smillie, Z., Esentia, I., Brackenridge, R., Xie, X., Bankole, S., Ducassou, E., Llave, E., 2020. Contourite porosity, grain size and reservoir characteristics. Mar. Pet. Geol. 117, 104392 https://doi.org/10.1016/j.marpetgeo.2020.104392.

Zenk, W., 1975. On the Mediterranean outflow west of Gibraltar. Meteor Forschungsergeb 16.